

Short title: α -glycosidase activity profiling

Corresponding author: Renier A. L. van der Hoorn

renier.vanderhoorn@plants.ox.ac.uk

Multiplex fluorescent, activity-based protein profiling identifies active α -glycosidases and other hydrolases in plants

Amjad M. Husaini¹, Kyoko Morimoto¹, Balakumaran Chandrasekar¹, Steven Kelly¹, Farnusch Kaschani², Daniel Palmero⁴, Jianbing Jiang³, Markus Kaiser², Oussama Ahrazem⁵, Hermen S. Overkleef³, Renier A. L. Van der Hoorn¹

¹ Department of Plant Sciences, University of Oxford, South Parks Road, Oxford OX1 3RB, United Kingdom.

² Chemische Biologie, Zentrum für Medizinische Biotechnologie, Fakultät für Biologie, Universität Duisburg-Essen, Universitätsstr. 2, 45117 Essen, Germany.

³ Gorlaeus Laboratories, Leiden Institute of Chemistry and Netherlands Center for Proteomics, Einsteinweg 55, 2333 CC Leiden, The Netherlands.

⁴ Universidad Politécnica de Madrid, Escuela Técnica Superior de Ingeniería Agronómica, Alimentaria cv de Biosistemas, Ciudad Universitaria s/n, 28040 Madrid, Spain

⁵ Instituto Botánico, Facultad de Farmacia, Universidad de Castilla-La Mancha, Campus Universitario s/n, Albacete 02071, Spain

One sentence summary: Activity profiling with biotinylated and fluorescent probes targeting α -glycosidases in plants is applied to saffron crocus and combined with other hydrolase probes.

Author contributions: AMH, KM, BC, RvdH designed the research; AMH, KM, BC performed research; DP, OA provided *Fox*-infected corms; FK, MK performed MS analysis; JJ, HSO contributed new analytic tools; SK generated the saffron proteome database; AMH, KM, BC, FK analyzed data; RvdH wrote the paper with input from all authors.

ABSTRACT

With nearly 140 α -glycosidases in 14 different families, plants are well equipped with enzymes that can break the α -glucosidic bonds in a large diversity of molecules. Here, we introduce activity-based protein profiling (ABPP) of α -glycosidases in plants using α -configured cyclophellitol aziridine probes carrying various fluorophores or biotin. In *Arabidopsis* (*Arabidopsis thaliana*), these probes label members of the GH31 family of Glycosyl Hydrolases, including ER-resident α -glucosidase-II RSW3/PSL5 (Radial Swelling-3/Priority for Sweet Life-5) and Golgi-resident α -mannosidase-II HGL1, both of which trim *N*-glycans on glycoproteins. We detected the active state of extracellular α -glycosidases such as α -xylosidase XYL1, which acts on xyloglucans in the cell wall to promote cell expansion, and α -glucosidase AGLU1, which acts in starch hydrolysis and can suppress fungal invasion. Labelling of α -glycosidases generates pH-dependent signals that can be suppressed by α -glycosidase inhibitors in a broad range of plant species. To demonstrate its use on a non-model plant species, we applied ABPP on saffron crocus (*Crocus sativa* L.), a cash crop for the production of saffron spice. Using a combination of biotinylated glycosidase probes, we identified and quantified 67 active glycosidases in saffron crocus stigma, of which ten are differentially active. We also uncovered massive changes in hydrolase activities in the corms upon infection with *Fusarium oxysporum* using multiplex fluorescent labelling in combination with probes for serine hydrolases and cysteine proteases. These experiments demonstrate the ease with which active α -glycosidases and other hydrolases can be analysed through ABPP in model and non-model plants.

Keywords: glycoside hydrolase, glycan, glucosidase, xylosidase, mannosidase, activity-profiling

INTRODUCTION

Carbohydrates in the form of glycoproteins, polysaccharides, and glycolipids play significant roles in cell physiology and development of plants, animals, and microbes. The enzymes that cleave and build the glycosidic bonds of glycoconjugates, oligosaccharides, and polysaccharides act on some of the most structurally diverse substrates in nature. Based on amino acid sequence similarity, these carbohydrate-active enzymes are classified into over 200 families of glycosidases, glycosyltransferases, carbohydrate esterases, and polysaccharide lyases in the carbohydrate-active enzyme database (CAZy; Coutinho et al. 1999).

Enzymes that catalyse the synthesis and breakdown of glycosidic bonds account for 1-3% of the proteins encoded by the genomes of most organisms. For instance, the genome of *Arabidopsis* (*Arabidopsis thaliana*) encodes for 400 glycosidases. These glycosidases play critical roles ranging from biosynthesis of glycoproteins to digestion and decomposition of polysaccharides. The α -glycosidases are an important subset of these enzymes. The CAZy database counts 138 α -glycosidases for *Arabidopsis*, subdivided into 14 families based on sequence homology (Lombard et al., 2013). These include α -galactosidases, α -amylases, α -xylosidases, α -rhamnosidases, α -fucosidases, α -threhalases, α -mannosidases, α -arabinofuranosidases, and α -glucosidases.

The Glycosyl Hydrolase 31 (GH31) family contains important α -glycosidases that act across the plant kingdom in protein *N*-glycosylation (RSW3 and HGL1), cell wall modulation (XYL1), and starch degradation (AGLU1). All GH31 family members are retaining α -glycosidases that retain the stereocenter of the C1 atom of the substrate with relatively large molecular weights (ca 100 kDa). Other α -glycosidases can be found in 13 additional GH families. Most of these glycosidases are inverting enzymes that invert the stereo centre of the C1 atom in the substrate. GH63, for example, contains the inverting α -glucosidase-I (GCS1, KNOPF), which resides in the ER, and removes the first glucose from the *N*-glycan of glycoproteins (Boisson et al., 2001). Plant α -glycosidases can have interesting properties. For instance, some α -glycosidases mediate the release of monoterpenoid aroma in apricots (Krammer et al., 2002). Furthermore, the α -glycosidase of the hyperthermophilic Archaeobacterium *Pyrococcus furiosus* remains active at 105-115°C (Constantio et al., 1990).

Many α -glycosidases can be blocked by selective inhibitors. Compounds like miglitol and acarbose are well-described α -glucosidase inhibitors used as anti-diabetic drugs (Hillman et al., 1989; Carrascosa et al. 2001). These compounds have occasionally been used to conduct research in plants; for instance, α -amylase was inhibited to study barley seed germination (Stanley et al., 2011, Frandsen et al., 2000). Iminosugars have also been used to study plant cell wall metabolism and starch remobilisation (Andriotis et al., 2017).

The large number of α -glycosidases, their complex regulation, and varied subcellular localisation call for new tools to detect when and where these enzymes are active. Activity-

based protein profiling (ABPP) is a simple and widely applicable technique that can display active enzymes in crude extracts and living tissues (Cravatt et al., 2008). ABPP is based on the use of small chemical probes that mimic a substrate but lock the enzymatic mechanism in the covalent intermediate state, labelling only active enzymes. Fluorescent probes facilitate the detection of the labelled proteome on protein gels by fluorescent scanning, whereas biotinylated probes facilitate the purification and identification of labelled proteins by mass spectrometry.

ABPP technology was initially developed in medical biology (Cravatt et al. 2008; Verhelst et al., 2005; Willems et al., 2014), and is increasingly used in microbiology (Sadler & Wright, 2015) and plant biology (Morimoto & Van der Hoorn, 2016). For instance, we have used activity-based probes to study the activities of the proteasome, serine hydrolases, cysteine proteases, glutathione transferases, aldehyde hydrogenases, metalloproteases, and ATP binding proteins in plants (Kaschani et al., 2009; Gu et al., 2010; 2013; Kolodziejek et al., 2011; Richau et al., 2012; Lenger et al., 2012; Misas-Villamil et al., 2013; 2017; Stiti et al., 2016). These probes have also been used by other plant research laboratories to investigate maize smut effectors, herbicide activation, wheat leaf senescence, and apical dominance in potato tubers (Gershater et al., 2007; Martinez et al., 2007; Mueller et al., 2013; Teper-Balnoelker et al., 2017).

We previously validated activity-based probes for retaining β -glycosidases in plants (Chandrasekar et al. 2014). Using β -configured cyclophellitol aziridine probes, we were able to monitor the activity of dozens of β -glycosidases, including β -myrosinases, β -glucosidases, β -xylosidases, and β -galactosidases (Chandrasekar et al. 2014). Here, we validate the use of α -configured cyclophellitol aziridine probes for retaining α -glycosidases in plants. These probes were recently developed and tested on mammalian proteomes (Jiang et al., 2016). We characterise the labelling profile, identify labelled proteins, and characterise the inhibitor-sensitivity of labelling. We also show their broad applicability for studying glycosidases in non-model plant species, exemplified by saffron, and demonstrate their use in combination with other fluorescent probes for profiling multiple classes of hydrolase activities simultaneously.

RESULTS

Distinct activity-based probes for α - and β -glucoside hydrolases

We studied the labelling of three different activity-based probes that carry a cyclophellitol-aziridine reactive group with glucopyranose in the α -configuration (**Fig. 1A**). This reactive group has been designed to target retaining α -glucoside hydrolases (α GHs, Jiang et al., 2016). The three probes used only differ in the reporter tag: JJB382 carries a Bodipy(FL) fluorophore; JJB383 a Cy5 fluorophore; and JJB384 a biotin affinity tag (Supplemental **Fig.**

S1). These probes are distinct from the probes introduced earlier, which contained β -configured cyclophellitol-aziridine reactive groups, aimed at labelling β -glucoside hydrolases (β GHs, Kallemeijn et al., 2012; Chandrasekar et al., 2014). The β -configured probes carry different reporter tags: KY371 carries an alkyne mini-tag; JJB70 a Bodipy(FL) fluorophore; JJB75 a Bodipy(TMR) fluorophore; and JJB111 a biotin affinity tag (**Fig. 1A**). When we previously tested these β -configured probes in plants, we found that they labelled a broad range of β GHs of the GH1, 3, 5, 30, 35, 51, 52 and 79 families, but not α GHs from GH31 (Chandrasekar et al., 2014).

The α -glucosidase probes label a distinct subproteome

To test the labelling by the new probes, Arabidopsis leaf extracts were labelled with JJB382 and JJB70, which differ in their reactive group configuration but have the same fluorophore. Labelled proteomes were separated on protein gels and detected by in-gel fluorescence scanning. The labelling profile of JJB382 is notably distinct from that described earlier for JJB70. Whilst JJB70 generates two strong signals at 70 kDa, caused by myrosinases TGG1 and TGG2 (Chandrasekar et al., 2014), JJB382 labelling does not display these signals. Instead, JJB382 labelling generates six signals (signals 1-6) at 100-130 kDa (**Fig. 1B** and Supplemental **Fig. S2**). These JJB382 signals 1-6 are 20-fold weaker than the JJB70 signals 8 and 9; therefore, high protein loading is required to detect the JJB382 signals robustly (**Fig. 1B** and **Fig. 1E**). Both JJB70 and JJB382 labelling also display a signal at 60 kDa (signal 7, **Fig. 1B**). Labelling with JJB382 causes a profile that seems identical to that of JJB383, indicating that the different fluorophores do not affect labelling (**Fig. 1C**).

Next, we tested the specificity of labelling in competition experiments. JJB383 labelling of signals 1-6 is suppressed upon pre-incubation with an excess of α -configured JJB384, but not β -configured KY371, indicating that signals 1-6 represent α GHs (**Fig. 1C**). However, JJB383 labelling of signal 7 is suppressed upon pre-incubation with β -configured KY371, but not α -configured JJB384, suggesting that this is a β GH-derived signal (**Fig. 1C**). Taken together, these experiments indicate that the α -configured fluorescent probes label a distinct set of proteins when compared to the β -configured probes.

Multiplex labelling of α - and β -glycosidases

Pre-labelling with β -configured JJB75 does not affect the labelling of signals 1-6 by α -configured JJB382 at 100-130 kDa (Supplemental **Fig. S3A**). However, JJB382 signal 7 at 60 kDa is suppressed upon pre-labelling with β -configured JJB75, consistent with this signal being generated by a β GH. Indeed, JJB75 labelling also generates a 60 kDa signal, similar to signal 10 of β -configured JJB70 (Supplemental **Fig. S3B** and **Fig. S3D**). Pre-labelling with JJB75 also generates an additional signal 8 at 70 kDa (Supplemental **Fig. S3A**), which might

result from unintended excitation of JJB75 at 488nm. JJB75-labelled proteins are also excited by the 633nm laser (Supplemental **Fig. S3C**), indicating that JJB75 cannot be used for co-labelling.

Conversely, pre-labelling with α -configured JJB383 does not affect β -configured JJB70 labelling (Supplemental **Fig. S3A**). The labelling profile of JJB383 (Supplemental **Fig. S3A**) is also identical to that of JJB382 (Supplemental **Fig. S3A**), except for the absence of signal 7, consistent with it being a β GH labelled by JJB70. Taken together, these data demonstrate that the α -configured probes cause distinct signals at 100-130 kDa, and that probes having different fluorophores can be used for co-labelling. Also, all fluorophores except for the Bodipy(TMR) of JJB75 are selectively detected using distinctive excitation and emission wavelengths.

The α -glycosidases have distinct labelling characteristics

The labelling experiments presented so far were performed at pH 7.0. Because α -glucosidases act in different subcellular locations with specific microenvironments, we tested labelling at various pH. JJB383 labelling is strongly pH-dependent. Labelling of signals 1-5 only occurs at pH 6.0 – 8.0, whilst labelling of signal 6 also occurs at pH 5.0 – 9.0 (**Fig. 2A** and **Fig. S4A**). In addition, signal 7 is most intense at pH 5.0, indicating that these β GHs act at acidic pH (**Fig. 2A** and **Fig. S4A**). The α GH-derived signals 1-5, however, are best labelled at neutral and slightly acidic pH (pH 6-8). To investigate whether the reduced α GH signals observed at low pH are caused by protein precipitation or degradation, we incubated a sample that was pre-labeled at pH 7.0 with JJB383 at various pH values. JJB383-labeled proteins were unaffected upon incubation at low pH (**Fig. 2A**, JJB383 panel), illustrating that α GH labelling is pH-dependent. Therefore, we focused further on α -glycosidase labelling at pH 7.0.

Next, we investigated the timing of JJB383 labelling. Signals 1-6 appear upon labelling within minutes and reach their maximum within 12 minutes (**Fig. 2B**). Signal 1, however, intensifies faster, indicating that this α GH has a higher turnover rate and is labelled faster by JJB383.

α -glucosidase inhibitors block labelling selectively

To confirm that the 100-130 kDa signals are generated by α -glucosidases, we tested labelling upon incubation with known α -glucosidase and control inhibitors. We tested two commercially available α -glucosidase inhibitors, acarbose and miglitol, which are used as anti-diabetic drugs (Hillman et al., 1989; Carrascosa et al., 2001). We also included the β -galactosidase inhibitor galactostatin, and three iminosugars that mimic glucose but differ stereochemically at the 5' and 4' positions: 1-deoxynojirimycin (DNJ), 1-deoxygalactonojirimycin (DGJ, migalastat), and *ido*-1-Deoxynojirimycin (*ido*DNJ) (**Fig. 3A**).

Pre-incubation with miglitol suppresses JJB383 labelling of signals 1-6 (**Fig. 3B**), indicating that these signals are caused by α -glycosidases. Surprisingly, acarbose does not affect labelling of signal 1 but suppresses labelling of signals 2-6 (**Fig. 3B**). Galactostatin is unable to prevent JJB383 labelling, indicating the relevance of the stereochemistry at the 1' and 4' positions (**Fig. 3B**). Of the tested iminosugars, DNJ and DGJ effectively block JJB383 labelling (**Fig. 3B**), indicating that the 4' stereochemistry is not essential for inhibiting JJB383 labelling. By contrast, *ido*DNJ is unable to block JJB383 labelling, indicating that the stereochemistry at the 5' position is essential for inhibiting JJB383 labelling. These results demonstrate that labelling of the 100-130 kDa proteins with α -configured probes is highly selective.

The 100-130 kDa signals contain four α -glycosidases

To identify the signals, we labelled Arabidopsis leaf extracts at pH 7.0 with biotinylated α -configured JJB384. We purified the biotinylated proteins and analysed them by in-gel and on-bead digests. For the in-gel digest procedure, purified JJB384-labelled proteins were separated on protein gels and stained with Sypro Ruby. Signals 1-6 that appear at 100-130 kDa in the JJB384-labelled sample, but not in the no-probe control, were excised and in-gel digested with trypsin (**Fig. 4A**). Released tryptic peptides were identified by LC-MS/MS. Four α -glycosidases were identified from all three excised signals: RSW3/PSL5 (Radial Swollen-3/Priority for Sweet Life-5, At5g63840, 36 spectral counts); α -xylosidase XYL1 (At1g68560, 17 spectral counts), HGL1 (Hybrid Glycosylation-1, At3g23640, 12 spectral counts), and α -glucosidase-1 AGLU1 (At5g11720, 10 spectral counts) (**Fig. 4B**). These four enzymes are GH31 α -glycosidases, and their predicted molecular weight (MW) is 104, 102, 111, and 101 kDa, respectively (**Fig. 4C**). These proteins can run at higher MW because they are likely *N*-glycosylated, as they have 2, 9, 3, and 9 putative *N*-glycosylation sites, respectively (**Fig. 4C**). We also identified a few peptides from the β -glucosidase BGLC3 (At5g04885, two spectral counts) from signals 4-6 (**Fig. 4A**, bands 4-5). However, this protein has a predicted MW of 68 kDa, and might be a contaminant from a different region of the gel.

Biotinylated α -glycosidase probes label 12 different α - and β -glycosidases

We also performed on-bead-digests to detect biotinylated proteins, and to determine if more proteins are labelled by JJB384. The pull-down was performed three times for JJB384-labelled proteins and three times for the no-probe-control (NPC). Of the 388 proteins detected, 33 were not from Arabidopsis, and 194 were not detected in more than two of the six samples (**Fig. 5A**). The average LFQ (Label-free Quantification) intensities for the 161 remaining proteins were plotted against their average distribution between the NPC and JJB384 samples.

As usual, the most abundant proteins are the endogenous biotinylated proteins BCCP, MCCA, and ACC1, as well as the highly abundant large Rubisco subunit RBCL (**Fig. 5B**, top signals). We also detect 12 proteins nearly exclusively in the JJB384 sample (**Fig. 5B**, right side), which are all glycosidases (**Fig. 5C**). We detected the same four GH35 α -glucosidases as with in-gel-digest: AGLU11, XYL1, HGL1, and RSW3. These four α -glucosidases are detected with high LFQ intensities and protein coverage, consistent with them being the preferred targets of JJB384. The remaining glycosidases are β -glycosidases of families GH116 (At4g10060), GH1 (BGLU15, -40, -42, and -44), and GH3 (F13I12, BGLC1 and -2) (**Fig. 5C**). The high spectral counts for BGLU44 and BGLC1 and their predicted MW suggest that these proteins might underlie signal 7, possibly mixed with other GH1 and GH3 enzymes. By contrast, our earlier pull-down analysis with β -configured JJB111 displayed most of the detected β -glycosidases, but none of the α -glucosidases (**Fig. 5C**, right). In conclusion, though JJB384 preferentially targets α -glucosidases, it also labels some but not all β -glycosidases. TGG1 and TGG2, for example, are abundant GH1 glucosidases in leaves but these were not detected among JJB384-labelled proteins.

Profiling of active α -glucosidases can be applied to other plant species

We next tested whether the α -configured probes can be used to detect α -glucosidases in leaf extracts of other plant species. In addition to Arabidopsis, we included a model legume (alfalfa, *Medicago sativa*), two solanaceous plants (*Nicotiana benthamiana*, and tomato, *Solanum lycopersicum*), two monocots (rice, *Oryza sativa*, and maize, *Zea mays*) and a gymnosperm (sago palm, *Cycas revoluta*). Pre-incubation with 50 μ M miglitol was used to distinguish between α - and β -glucosidases. Labelling causes fluorescent signals at 10-130 kDa for all the plant species tested; these signals are suppressed upon miglitol pre-incubation, and absent in the no-probe-control (**Fig. 6**). The signals are similar in intensity and molecular weight, though there are slight differences in the profiles. Signals at 40-60 kDa are not suppressed upon pre-incubation with miglitol, indicating that these are generated by β -glucosidases (**Fig. 6**). In conclusion, these α -configured probes can be used to monitor miglitol-sensitive α -glucosidases in various plant species.

Glycosidase activity profiling of a non-model: saffron crocus anthesis

We next used glycosidase activity profiling to investigate anthesis in *Crocus sativus*, the saffron crocus. The stigma of these monocot flowers are harvested, dried, and widely used as a spice and for food coloring (Ahrazem et al., 2015). During the drying process, heat, and presumably glucosidases, convert the bitter tasting picrocrocin into glucose and safranal, which gives saffron its distinct aroma (Jain et al., 2016). The glycosidases catalysing this

reaction, and the conversion of other volatiles and non-volatile apocartenoids, have not been identified.

To initiate the characterisation of safranal-generating glucosidases, we performed glucosidase activity profiling at two different stages of stigma development and maturation: yellow (stage-1) and scarlet (stage-4) (Wafai et al. 2016). Taking advantage of having different fluorophores on α - and β -configured probes, we simultaneously monitored active α - and β -glucosidases using multiplex fluorescence. As with other plant species, the α -configured probe JJB383 displays signals at 100-130 kDa, which do not change in intensity during anthesis (**Fig. 7A**). By contrast, the β -configured JJB70 displays a constant signal at 70 kDa, and a differential signal at 110 kDa that is particularly strong at stage-4 (**Fig. 7A**). This 110 kDa signal overlaps with the JJB383-derived signals, causing a purple signal in the overlay image (**Fig. 7A**).

To determine if the 110 kDa glycosidase is labeled by both JJB383 and JJB70, or if these signals are generated by two different labeled glycosidases that co-migrate, we preincubated the samples with the α GH inhibitor miglitol and the β GH inhibitor KY371. The JJB70-labeled 110 kDa signal is only suppressed by KY371, and the JJB383-labeled signals are only suppressed by miglitol (**Fig. 7A**). This result demonstrates that the labeled GHs are co-migrating, and that the differential signal is a β GH.

To identify glucosidases that are differentially active between stages -1 and -4, we performed labelling with mixed, biotinylated probes targeting both α - and β -glycosidases (JJB384 and JJB111, respectively). Labelling was performed on three biological replicates, both from stage-1 and stage-4 samples, and peptides from on-bead trypsin digests were identified. To facilitate the annotation of MS spectra, we annotated the proteome based on published RNAseq data of *Crocus sativus* (Jain et al., 2016). We detected and quantified 67 putative glycosidases (**Fig. 7B**) and plotted their relative occurrence in stages-1 and -4 against the predicted molecular weight (**Fig. 7B**).

Four of the detected glycosidases are putative orthologs of Arabidopsis XYL1, RSW3, and AGLU1, of the GH31 family. However, these α GHs are not differentially active (**Fig. 7B**, blue circles), consistent with the unaltered fluorescent labelling profiles (**Fig. 7A**). In addition to GH31 glycosidases, we also detected peptides from representatives of eight additional GH families: GH1 (21x), GH35 (15x), GH3 (12x), GH116 (10x), GH31 (4x), GH17 (2x), GH2 (1x), GH5 (1x), and GH27 (1x).

Of the 67 active glycosidases that we could quantify, eight were significantly upregulated more than 2-fold in stage-4 stigma (**Fig. 7B**, right, encircled), including three GH3, three GH35, two GH116, and one GH1. One GH1 glycosidase with a predicted MW of 130 kDa was significantly downregulated more than two-fold when compared to stage-4 stigma (**Fig. 7B**, left, encircled). We also note the enrichment of several additional GH1

glycosidases in stage-4 stigma, albeit not statistically significant (**Fig. 7B**, green circles). The differential 110 kDa β GH detected with JJB70 labeling is likely the GH116 enzyme CsTc017194, because this enzyme has a predicted molecular weight of 106 kD and is 4.5-fold upregulated in stage-4 stigma (**Fig. 7B**, left top purple circle). This experiment illustrates the power of applying quantitative glycosidase activity profiling on non-model plant species.

Multiplex activity profiling displays changed hydrolase activities in *Fox*-infected corms

To illustrate the combination of glycosidase activity profiling with activity profiling of other enzyme classes, we investigated infections of saffron corms with *Fusarium oxysporum* (*Fox*). *Fusarium* corm rot caused by *Fox* is the most destructive disease in saffron, having caused severe yield losses in saffron producing countries (Cappelli et al., 1994; Husaini et al., 2014). *Crocus sativus* corms were infected with four different *Fox* isolates, including three different *formae speciales* (Palmero et al. 2014), and analysed for differential protein activities at three weeks after infection.

By combining probes having different fluorophores, we were able to display a large number of active hydrolases in only two labelling reactions on multiple biological replicates. The combination of JJB383 and FP-Tamra displays α -glycosidase and serine hydrolases using different fluorophores, respectively. Likewise, the combination of JJB70, MV201, and JOPD1 displays the activities of β -glycosidases and cysteine proteases using different fluorophores. These experiments displayed remarkably different profiles upon infection, irrespective of the *Fox* isolate used (**Fig. S5**). Activities of both 100 kDa putative α -glucosidase and putative β -glucosidases at 50-70 kDa are increased upon infection (**Fig. 8A**). By contrast, the activity of one strong 50 kDa and several weaker 60 kDa serine hydrolase signals is reduced upon infection (**Fig. 8B**). Several active β -glucosidases of 45-60 kDa appear upon infection, whilst strong signals at 65 and 70 kDa disappear (**Fig. 8C**). Finally, the activity profile of cysteine proteases changes dramatically upon infection (**Fig. 8D**). These signals represent papain-like cysteine proteases (PLCPs, MV201, Richau et al., 2012) or vacuolar processing enzymes (VPEs, JOPD1, Lu et al., 2015). In conclusion, this simple experiment illustrates the ease and potential of investigating the activities of diverse classes of hydrolases using probes having different fluorophores.

DISCUSSION

We have validated activity-based probes for α -glycosidases in plants. We discovered that they label all four members of the GH31 family, as well as many additional β -glycosidases that run at a lower MW. The labelling of α -glycosidases is pH-dependent, and can be suppressed by miglitol and partially by acarbose. Activity profiling of α -glycosidases can be broadly applied

to other plants, including non-model plant species. We used glycosidase probes to quantify and identify 67 active glycosidases from the stigma of the saffron crocus. We also used multiplex fluorescent labelling with probes for serine hydrolases and cysteine proteases to display the dynamics of hydrolase activities in crocus corms upon infection with *Fusarium oxysporum*.

The range of enzymes labelled by α -glycosidase probes

We detected four GH31 α -glycosidases in Arabidopsis, both by in-gel and on-bead digest of purified biotinylated proteins (**Fig. 4** and **Fig.5**). We also identified the putative orthologs of three of the active GH31 α -glycosidases from the non-model plant species saffron crocus (**Fig. 7**), illustrating the robustness of α -glycosidase activity in different plant species. Although we did not detect XYL2, the gene encoding XYL2 is considered a pseudogene (Iglesias et al., 2006).

It is interesting to note that although our probes mimic α -glucose, consistent with the labelling of the α -glucosidases AGLU1 and RSW3, we also label glycosidases that recognise α -xylose (XYL1) and α -mannose (HGL1). These two monosaccharides are, however, relatively similar to glucose. This result indicates that the α -configured cyclophellitol aziridine probes have a degree of promiscuity, allowing them to label a broad range of glycosidases. We made a similar observation for the β -configured cyclophellitol aziridine probes that not only label β -glucosidases, but also β -galactosidases, β -xylosidases, β -glucuronidases, and β -glucanases (Chandrasekar et al., 2014).

We did not detect α -glycosidases from other GH families for several reasons. First, the majority of the other α -glycosidases are inverting glycosidases, and these do not covalently react with cyclophellitol aziridine probes. These include the ER-resident α -glucosidase-I (GCS1, KNOPF) that catalyses the first step of *N*-glycan trimming in the folding cycle, and is a GH63 inverting α -glycosidase (Boisson et al., 2001). Second, the α -configured cyclophellitol aziridine probe may not be able to enter more specific substrate binding pockets of α -glycosidases acting on complex glycans. Third, not all α -glycosidases may be expressed in the analysed tissues, or may not be active under the tested conditions. This condition-dependency is illustrated by the fact that the labelling profile depends on pH (**Fig. 2**).

In addition to α -glycosidases, we also detected the labelling of a large number of β -glycosidases. This result is remarkable because the α -glycosidases were not detected with β -configured probes (Chandrasekar et al., 2004). However, this may be due to the lower concentration of α -glycosidases when compared to β -glycosidases. Nevertheless, the fact that α -configured probes label β GHs, but not *vice versa*, has also been noted in studies on mammalian proteomes (Jiang et al., 2016), and this property has been used to design more

selective α GH inhibitors (Artola et al., 2017). Interestingly, not all β -glycosidases are labelled by α -configured probes. The highly abundant myrosinases TGG1 and TGG2, for example, produce strong labelling signals with β -configured probes (Chandrasekar et al., 2014 and **Fig. 1B**), but are not labelled by the α -configured probes and not detected by MS.

The identity of the 100-130 kDa signals in the α -glycosidase activity profiles

The α -glycosidases cause distinct signals in the 100-130 kD region, consistent with their predicted molecular weight (**Fig. 4**). Unfortunately, the signals are too close to separate and identify the proteins corresponding to each signal. However, we can predict that the bottom signals represent AGLU1 and XYL1 for several reasons. First, this signal also appears upon labelling at pH 4.0 – 5.0 (**Fig. 2A**), consistent with their function in the apoplast. Second, this signal is sensitive to acarbose inhibition (**Fig. 3**), and AGLU1 is known to be inhibited by acarbose (Frandsen et al., 2000). Third, AGLU1 and XYL1 have the lowest predicted MW (**Fig. 5C**). Conversely, our data suggest that HGL1 may generate one of the top signals, as it is expected to have higher MW and to be active in the Golgi (pH 6.5). This result implies that HGL1 may be insensitive to acarbose but not miglitol inhibition.

α -glycosidase activity profiling is broadly applicable in plant science

Our work demonstrates that α -glycosidase activity profiling is broadly applicable. We were able to display miglitol-sensitive labelling of 100-130 kDa proteins from leaves of monocot and dicot plants and the though leaves of a gymnosperm (**Fig. 6**). These signals very likely represent the orthologs of the Arabidopsis α -glycosidases RSW3, HGL1, AGLU1, and XYL1. Three of these enzymes were also detected upon labelling of saffron crocus anthers (**Fig. 5C**). We displayed activity profiles of α -glycosidases in leaves, stigma, and corms (**Figs. 6-8**), further supporting the broad applicability of this technique. Since the probes are uncharged, and β -configured probes have been used for *in vivo* labelling (Chandrasekar et al., 2014), we believe that the probes can also be used for *in vivo* labelling of α -glycosidases.

We also applied α -glycosidase activity profiling to stigma and corms of the saffron crocus to study stigma development (**Fig. 7**) and *Fox* infection (**Fig. 8**). These experiments illustrate the ease by which α -glycosidase activity profiling can be applied to cash-crop plants to generate data for follow-up studies. For instance, our data suggest candidate glycosidases responsible for the conversion of picrocrocin into safranal in harvested stigma. Likewise, we detect the suppressed activity of an α -glycosidase upon infection with *Fox*, consistent with the notion that *Fox* is likely to suppress AGLU1 in the apoplast during infection to overcome the antifungal activity of this enzyme (Monroe et al., 1999; Xiao et al., 1994).

Multiplex fluorescence activity profiling display dynamic changes in hydrolase activities

The use of probes having different fluorophores greatly expands the ease by which we can profile multiple classes of hydrolases simultaneously. Multiplex labelling will drastically accelerate research and miniaturise the experiments. By labelling of saffron stigma and infected corms (**Fig. 7A** and **Fig. 8**), we have illustrated the ease by which multiplex fluorescence simultaneously displays activity profiles of different enzyme classes.

The changes in hydrolase activities upon infection of corms by *Fox* are interesting and robust (**Fig. 8** and **Fig. S5**). The signals that appear in infected corms may be generated by plant-produced hydrolases aimed to suppress the disease, or come from *Fox* itself, to macerate the host tissue (Mohamed et al., 2017). The reduced activity of a 50 kDa plant serine hydrolase upon *Fox* infection may be caused by a depletion of this 50 kDa protein, but may also be caused by the suppression of the activity of this protein by *Fox*. We have detected a similar suppression of host hydrolase activities upon bacterial infection (Hong et al., 2014; Chandrasekar et al., 2017). The suppression of host enzymes can be further studied using convolution ABPP, where samples from infected and noninfected samples are mixed before and after labelling (Chandrasekar et al., 2017).

In conclusion, we have validated activity profiling for α -glycosidases, showed its broad applicability by profiling other tissues, plant species and biological phenomena, and introduced multiplex labelling to speed up and miniaturise activity profiling in plant science.

MATERIAL AND METHODS

Used probes and inhibitors – Activity-based probes JJB382, JJB347, JJB383, JJB384 (Jiang et al., 2016) and JJB70, JJB75, JJB111, KY371 (Kalemeijn et al., 2012; Chandrasekar et al., 2014) have been described previously. Immunosugars DNJ (Wennekes et al., 2007), DGJ and idoDNJ (Wennekes et al., 2010) have been described previously. Acarbose, Miglitol, Galactostatin were purchased from Sigma-Aldrich, Tocris, and Santa Cruz, respectively.

Plant material, growth conditions, and *Fox* infections - *Arabidopsis thaliana* (L) Heynh. ecotype Columbia, *Medicago sativa*, *Nicotiana benthamiana*, *Solanum lycopersicum*, *Oryza sativa*, *Zea mays*, and *Cycas revoluta* were grown on soil under standard greenhouse conditions. Healthy corms of saffron previously disinfected with 5% sodium hypochlorite for 15 min., followed by three washes with sterile water, were planted in sterile substrate and held for 3 weeks with controlled temperature and light (12/12 h light/dark, 25/21°C). The inoculum consisted of a suspension of conidia obtained after a week in potato–glucose medium, stirred at 150 rpm. To remove the mycelium, the suspension was filtered with a double layer of cheesecloth. The conidia suspension was adjusted to 10^5 conidia/mL and used

for inoculation of plant material. The plant roots were immersed for 24 h in the suspension of conidia (200 mL suspension), then transplanted back and kept under the same conditions of temperature and light for 3 weeks.

Protein extraction - Two leaf discs (0.9-cm diameter) were taken from the leaves of various plant species and homogenized with 300 µl of a buffer with suitable pH (50 mM sodium acetate buffer for pH 3.0 and 4.0, 50 mM MES buffer for pH 5.0 and 6.0, 50 mM MOPS buffer for pH 7.0 and 8.0, 50 mM Tris buffer for pH 9.0 and 10). After the tissues had been ground in a 1.5-ml tube, the samples were centrifuged at 10,000 g (4 °C for 10 min) followed by 11,000 g (4 °C for 5 min) to remove cell debris, and the supernatant containing soluble proteins was used for labelling.

Labelling plant extracts - All probes were prepared as 0.1-10 mM stock solutions in dimethyl sulfoxide (DMSO). Equal volumes of DMSO were used as no probe control. Labelling was performed as described previously (Chandrasekar et al., 2014). For fluorescence gel imaging, the extracts were incubated with 2 µM probes for 1h at room temperature in the dark at 50 µl total reaction volume. For the competition experiments, the extracts were pre-incubated with the corresponding inhibitors at 50 µM for 30 min prior to labelling with the probe.

The labelling reactions were quenched by adding 4 x gel loading buffer (200 mM Tris-HCl (pH 6.8) 400 mM dithiothreitol (DTT), 8% (w/v) SDS, 0.04% (w/v) bromophenol blue, 40% (v/v) glycerol) at 1 x final concentration and heating at 95 °C for 5min. The labelled proteins were separated on 10% protein gels and detected in the protein gels with the Typhoon FLA 9000 scanner at excitation 488 nm and emission 520 nm (ex488/em520) or ex633/em670 (GE Healthcare Life Sciences). Subsequent to fluorescent imaging, the gels were stained with Coomassie brilliant blue R-250. The fluorescence of the labelled proteins was quantified using ImageJ. For pull-down experiments, the extracts from three biological replicates were incubated with 5 µM probes for 1.5 h at room temperature in the dark at 1 mL total reaction volume. The labelling reactions were quenched by precipitating the total proteins via the chloroform/methanol precipitation method (Wessel and Flugge, 1984).

Pull-down and on-bead, in-gel trypsin digestion - Pull-down experiments and on-bead and in-gel trypsin digestions were performed as described with minor modifications (Chandrasekar et al., 2014). For Arabidopsis, healthy leaf discs (1.5 gm) were collected from middle/top leaves of 5-week old Arabidopsis plants growing in different pots at the same point of time. Leaf disks were mixed and three separate extracts were generated in 50 mM MOPS at pH 7.0. For saffron sigma, four stigmas, each from a single flower, were harvested

for each stage from different plants of the same age but at different time points. These four stigma were pooled for pulldown experiment and three of these pooled samples were used as biological replicates. The trypsin-digested peptides were purified using Sep-Pak C18 columns (Waters, WAT020515). Columns were equilibrated with 2% (v/v) acetonitrile (ACN), 0.1% (v/v) formic acid (FA) before peptides loading. Peptides were washed with 10 ml of 2% (v/v) ACN, 0.1% (v/v) FA and eluted with 2×1 mL of 65% (v/v) ACN, 0.1% (v/v) FA. Purified peptides were dried in a vacuum centrifuge and subjected to Mass Spectrometry analysis. After elution from the SEP-Pak, samples were dried using a vacuum concentrator (Eppendorf), and the peptides were resuspended in 0.1 % formic acid solution (15 μ L).

LC-MS/MS - Experiments were performed on an Orbitrap Elite instrument (Thermo, Michalski et al., 2012) that was coupled to an EASY-nLC 1000 liquid chromatography (LC) system (Thermo). The LC was operated in the one-column mode. The analytical column was a fused silica capillary (75 μ m \times 20 cm or 75 μ m \times 40 cm) with an integrated PicoFrit emitter (New Objective) packed in-house with Reprosil-Pur 120 C18-AQ 1.9 μ m resin (Dr. Maisch). The analytical column was encased by a column oven (Sonation) and attached to a nanospray flex ion source (Thermo). The column oven temperature was adjusted to 45 °C during data acquisition and in all other modes at 30 °C. The LC was equipped with two mobile phases: solvent A (0.1% formic acid, FA, in water) and solvent B (0.1% FA in acetonitrile, ACN). All solvents were of UPLC grade (Sigma). Peptides were directly loaded onto the analytical column with a maximum flow rate that would not exceed the set pressure limit of 980 bar (usually around 0.6 – 1.0 μ L/min). Peptides were subsequently separated on the analytical column by running a 70 min or 140 min gradient of solvents A and B (70 min gradient: start with 7% B; gradient 7% to 35% B for 60 min; gradient 35% to 100% B for 5 min and 100% B for 5 min; 140 min gradient: start with 7% B; gradient 7% to 35% B for 120 min; gradient 35% to 100% B for 10 min and 100% B for 10 min) at a flow rate of 300 nl/min. The mass spectrometer was operated using Xcalibur software (version 2.2 SP1.48). The mass spectrometer was set in positive ion mode. Precursor ion scanning was performed in the Orbitrap analyzer (FTMS; Fourier Transform Mass Spectrometry) in the scan range of m/z 300-1800 and at a resolution of 60000 with the internal lock mass option turned on (lock mass was 445.120025 m/z, polysiloxane (Olsen et al., 2005)). Product ion spectra were recorded in a data-dependent fashion in the ion trap (ITMS) in a variable scan range and at a rapid scan rate. The ionization potential (spray voltage) was set to 1.8 kV. Peptides were analyzed using a repeating cycle consisting of a full precursor ion scan (1.0×10^6 ions or 50 ms) followed by 12 or 15 product ion scans (1.0×10^4 ions or 80 – 100 ms) where peptides are isolated based on their intensity in the full survey scan (threshold of 500 counts) for tandem mass spectrum (MS2) generation that permits peptide sequencing and identification. Collision-induced

dissociation (CID) energy was set to 35% for the generation of MS2 spectra. During MS2 data acquisition dynamic ion exclusion was set to 60 – 120 seconds with a maximum list of excluded ions consisting of 500 members and a repeat count of one. Ion injection time prediction, preview mode for the FTMS, monoisotopic precursor selection and charge state screening were enabled. Only charge states of > 1 were considered for fragmentation.

Peptide and Protein Identification using MaxQuant - Spectra (RAW files) were submitted to an Andromeda (Cox et al., 2011) search in MaxQuant (version 1.5.0.25 or 1.5.3.30) using the default settings (Cox et al., 2008). Label-free quantification and match-between-runs were activated (Cox et al., 2014). For Arabidopsis samples, the MS/MS spectra data were searched against an *Arabidopsis thaliana* (mouse-ear cress, taxonomy-id: 3702) database downloaded from the TAIR repository (TAIR10_pep_20110103.fasta; 27416 entries). For Saffron (*Crocus sativus* L, taxonomy-id: 82528) samples, we generated a dedicated protein database by translating the publicly available RNA-Seq data from Jain et al. (2016) and filtering for open reading frames that encode proteins >50 amino acids (Saffron.PROTEIN_50.fasta; 83422 entries). All searches included a contaminants database search (as implemented in MaxQuant, 245 sequences). The contaminants database contains known MS contaminants and was included to estimate the level of contamination. Andromeda searches allowed oxidation of methionine residues (16 Da) and acetylation of the protein N-terminus (42 Da) as dynamic modifications and the static modification of cysteine (57 Da, alkylation with iodoacetamide). Enzyme specificity was set to “Trypsin/P” with two missed cleavages allowed. The instrument type in Andromeda searches was set to Orbitrap, and the precursor mass tolerance was set to ± 20 ppm (first search) and ± 4.5 ppm (main search). The MS/MS match tolerance was set to ± 0.5 Da. The peptide spectrum match FDR and the protein FDR were set to 0.01 (based on target-decoy approach). Minimum peptide length was seven amino acids. For protein quantification, unique and razor peptides were allowed. Modified peptides were allowed for quantification. The minimum score for modified peptides was 40. Label-free protein quantification was switched on, and unique and razor peptides were considered for quantification with a minimum ratio count of 2. Retention times were recalibrated based on the built-in nonlinear time-rescaling algorithm. MS/MS identifications were transferred between LC-MS/MS runs with the “Match between runs” option, in which the maximal match time window was set to 0.7 min and the alignment time window set to 20 min. The quantification was based on the “value at maximum” of the extracted ion current. At least two quantification events were required for each protein. Further analysis and filtering of the results was done in Perseus v1.5.5.3 (Tyanova et al., 2016). Briefly, only protein groups with at least two identified unique peptides over all runs were considered for further analysis. Comparison of protein group quantities (relative quantification) between different MS runs

was based solely on the LFQs, as calculated by MaxQuant (MaxLFQ algorithm, Cox et al., 2014). Imputed values were generated over the whole matrix, and the fold change and p-values were calculated over the three biological replicates.

Open reading frame detection and domain annotation - The complete set of *de novo* assembled transcripts were subject to open reading frame detection using three different prediction algorithms; GeneMarkS-T (Tang et al. 2015), TransDecoder (Haas et al. 2013), and Prodigal (Hyatt et al. 2010). Prodigal was run in both intronless eukaryotic and prokaryotic modes; thus, up to four open reading frame predictions were generated for each transcript. To select the single, best open reading frame for each transcript, the following process as applied. If multiple methods predicted overlapping open reading frames, then the longest was chosen. Where multiple methods disagreed on the correct open reading frame, then the following decision process was followed. If all methods disagreed (either in frame or location), then the priority for assignment was taken as GeneMarkS-T, TransDecoder, Prodigal (eukaryotic settings), Prodigal (prokaryotic settings). If some methods agreed, then the open reading frame that was detected by the largest number of methods was chosen. Only open reading frames ≥ 50 amino acids were selected for further analysis. To annotate conserved domains in the predicted open reading frames, the full PFAM-A database (Finn et al. 2016) was searched against the complete set of open reading frames with an e-value cut-off of $1e-5$.

Data Availability

The mass spectrometry proteomics data have been deposited to the ProteomeXchange Consortium via the PRIDE (Vizcaíno et al. 2016) partner repository with the dataset identifier PXD009014". During review, data can be accessed via a reviewer account (Username: reviewer04655@ebi.ac.uk; Password: CCmqkMNZ). The samples are named as follows: in-gel digests Arabidopsis leaves [ACE0111: bands 1-4 (AH7-9)]; on-bead digest Arabidopsis leaves [ACE0149: JJB384 (AH2,5,8) and no-probe control (AH1,4,7)]; and on-bead digest Saffron stigma [ACE0158: Stage-1 (AS13-15), Stage-4 (AS3-6) and no-probe control (AS1-3)].

Accession Numbers

At5g11720 (AGLU1), At5g63840 (RSW3/PSL5), At3g23640 (HGL1), At1g68560 (XYL1), At4g10060 (GH116), At2g44450 (BGLU15), At1g26560 (BGLU40), At5g36890 (BGLU42), At3g18080 (BHLU44), At3g47000 (F13I12), At5g20950 (BGLC1), At5g04885 (BGLC3).

Supplemental Data

Supplemental Figure 1. Structures of the probes used.

Supplemental Figure 2. Activity profiles of α - and β -glucosidase probes.

Supplemental Figure 3. Subsequent labelling of α - and β -glucosidases.

Supplemental Figure 4. Duplicate of pH course.

Supplemental Figure 5. Replicates of *Fusarium* infection of saffron corms.

Supplemental File S1. The saffron protein database.

Acknowledgments

This work was financially supported by Department of Biotechnology of the Government of India (AMH); ERC Consolidator grant 616449 ‘GreenProteases’ (RvdH); John Fell Fund (KM); ERC starting grant (MK, grant No. 258413), the Deutsche Forschungsgemeinschaft (MK, grant No. INST 20876/127-1 FUGG), and the China Scholarship Council (JJB, grant No. 2011618045). We like to thank Ursula Pyzio for excellent plant care.

Figure Legends

Figure 1 α -glucosidase probes label distinct proteins in Arabidopsis leaf extracts.

(A) Structures of the probes used for α -glucosidases (top) and β -glucosidases (bottom). For the detailed structures, see **Supplemental Figure S1**. (B-E) Activity profiles of α - and β -glucosidase probes. Arabidopsis leaf extracts at pH 7.0 were pre-incubated with or without 50 μ M JJB384 (384) or KY371 (KY) for 30 minutes and then labelled with or without 2 μ M JJB382 (382), JJB383 or JJB70 for one hour. Proteins were separated on protein gels and analysed by in-gel fluorescence scanning at excitation 488nm and emission 520nm (ex488/em520) (B) or ex633/em670 (C) and overlaid (D), and Coomassie stained (E). Four times less JJB70-labelled sample was loaded to compare JJB70 and JJB382 profiles. For full gels, see **Supplemental Figure S2**.

Figure 2 pH-dependency and time course of α -glucosidase labelling.

(A) Arabidopsis leaf extracts were labelled with 2 μ M JJB383 for one hour at pH7. This sample was buffer exchanged with water, followed by mixing with an unlabeled proteome plus 2 μ M JJB383 and labeled for one hour at various pH values. Proteins were precipitated with acetone and analyzed by in-gel fluorescence scanning at 488nm excitation and 520nm emission (ex488/em520) for JJB382 (top panel); ex633/em670 for JJB383 (second panel) and coomassie (CBB) staining (bottom). The overlay (third panel) shows JJB382 in red and JJB383 in blue.

(B) Quantified time course of α -glucosidase labelling of Arabidopsis leaf extracts.

Arabidopsis leaf extracts were labelled with 2 μ M JJB383 at pH 7.0 and samples were

649 collected at various time points. The Y axis displays fluorescence intensities from protein gels,
650 the X axis indicates time (minutes).

Figure 3 JJB383 labelling is blocked by α -glucosidase inhibitors.

(A) Glycosidase inhibitors used in this study. (B) Competitive ABPP using glycosidase inhibitors. Arabidopsis leaf extracts were pre-incubated with and without 50 μ M inhibitors and labelled with 2 μ M JJB383 for one hour at pH 7.0. Samples were analyzed by in-gel fluorescence scanning (ex633/em670, top) and Coomassie staining (bottom).

Figure 4 100-130 kDa region contains four α -glucosidases.

(A) Arabidopsis leaf extracts were labelled with and without 5 μ M JJB384 for one hour at pH 7.0. Biotinylated proteins were purified on high capacity streptavidin agarose resin beads and eluted by boiling in SDS sample buffer. Proteins were separated on protein gels and stained with Sypro Ruby. Gel slices were excised, treated with trypsin and released peptides analysed by LC-MS/MS. (B) Five glycosidase proteins were identified in bands 1-6. (C) Detected proteins and their domain structure; predicted molecular weight (MW, in kDa); and number of putative N-glycosylation sites (PGS).

Figure 5 On-bead digests identifies 12 α - and β -glycosidases.

(A) Selection criteria for pull-down proteomics. Arabidopsis leaf extracts were labelled with and without 5 μ M JJB384 and biotinylated proteins were purified on high capacity streptavidin agarose resin beads. On-bead digests with trypsin were analyzed by MS and Arabidopsis proteins that were detected in three of the six pull-down experiments were selected.

(B) Distribution of the detected proteins over the no-probe-control and JJB384-labelled sample. The average LFQ scores were plotted against the distribution of the LFQ scores for each protein detected with and without the probe. All 12 highly enriched proteins are glycosidases, highlighted on the right. Abundant, non-enriched signals come from endogenously biotinylated proteins (BCCP, MCCA and ACC1) and the large subunit of RuBisCo (RBCL). NPC, no-probe-control.

(C) Characterization of the detected probe targets. We detected four GH1 glycosidases (green), three GH3 glycosidases (red), four GH31 glycosidases (blue) and one GH116 glycosidase (purple), each with unique (black, u) and ambiguous (grey, a) peptides, summarised in columns 'u' and 'a' respectively. The presence of a signal peptide (SP, SignalP prediction), the predicted Molecular Weight (MW, in kDa) and number of putative N-glycosylation sites (PGS, NxS/T) are indicated. α/β , annotation as α - or β -glycosidase; JJB111, detected previously in β -glycosidase pull-downs (Chandrasekar et al., 2014).

Figure 6 α -glucosidase profiling in leaves of other plant species.

Leaf extracts were pre-incubated with or without 50 μ M miglitol and then labelled with or without 2 μ M JJB383 at pH 7.0 for one hour. Samples were analysed by in-gel fluorescence

scanning (ex633/em670, top) and Coomassie staining (bottom). *At*, *Arabidopsis thaliana*; *Ms*, *Medicago sativa*; *Nb*, *Nicotiana benthamiana*; *Sl*, *Solanum lycopersicum* (tomato); *Os*, *Oryza sativa* (rice); *Zm*, *Zea mays* (maize); *Cr*, *Cycas revolute* (sago palm). Putative α GH signals are suppressed by miglitol preincubation (white dots) whereas putative β GH signals are not (black dots).

Figure 7 Glucosidase activities in the stigma of *Crocus sativus* during anthesis .

(A) Glycosidase activity profiles of stigma at anthesis stages 1 and 4. Stigma extracts of stages 1 and 4 were preincubated at pH 7.0 with and without 50 μ M miglitol or KY371 for 30 minutes and then labelled with or without 2 μ M JJB383 or JJB70 for one hour. The JJB383- and JJB70-labeled samples were mixed and separated on protein gels, and analysed by in-gel fluorescence scanning at ex633/em670 for JJB383 (top panel) and ex488/em520 for JJB70 (second panel), and coomassie staining (bottom panel). The overlay (third panel) shows JJB383 labeling in blue and JJB70 labeling in green.

(B) Comparative glycosidase activity profiling of stages 1 and 4 stigma of *Crocus sativus*. Stigma extracts of stages 1 and 4 were labelled with or without 5 μ M biotinylated probes in triplicate, and biotinylated proteins were purified on avidin beads. On-bead trypsin digests were analysed using a re-annotated proteome of *Crocus sativus*. For each detected glycosyl hydrolase, the occurrence in the two samples (ratio) was plotted against the predicted molecular weight, with the circle size representing the p-value and the color indicating the GH family. Ten significantly differential GHs ($p < 0.01$, Students *t*-test) are highlighted with a black edge.

Figure 8 Differential hydrolase activities in Saffron corms upon infection with *Fusarium oxysporum* (*Fox*).

Saffron corms were inoculated with or without four different *Fox* isolates in duplicate (Supplemental **Figure S5**) and cell free extracts were generated and lyophilized after two weeks. Extracts were labelled for 4 hrs in 4 mM DTT at pH 7.0 with 2 μ M JJB383 and FP-Tamra (**A, B**), or at pH 5.0 with 2 μ M JJB70, MV201 and JOPD1 (**C, D**), respectively. Proteins were separated on protein gels and analysed by in-gel fluorescence scanning at ex633/em670 to detect JJB383 (**A**), ex488/em520 to detect JJB70 (**C**), ex532/em610 to detect FP-Tamra, MV201 and JOPD1 (**B, D**). The bottom panels show the overlay of JJB383 in blue and FP-Tamra in red (left) and JJB70 in green and MV201+JOPD1 in red (right) and Coomassie staining (bottom). Shown are the mixed Mock and *Fox* samples in duplicate, and a mix of the mixed proteomes as no-probe-control (mix). Activity profiles of separate proteomes are shown in Supplemental **Figure S5**.

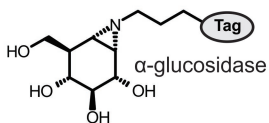
REFERENCES

- Andriotis VME, Rejzek M, Barclay E, Rugen MD, Field RA, Smith AM (2017) Cell wall degradation is required for normal starch mobilisation in barley endosperm. *Sci. Rep.* **6**: 33215
- Ahrazem O, Rubio-Moraga A, Nebauer SG, Molina RV, Gómez-Gómez L (2015) Saffron: its phytochemistry, developmental processes, and biotechnological prospects. *J Agric Food Chem* **63**: 8751-8764
- Artola M, Wu L, Ferraz MJ, Kuo CL, Raich L, Breen IZ, Offen WA, Codee JDC, Van der Marel G, Rovira C, Aerts JMFG, Davies GJ and Overkleeft HS (2017) 1,6-cyclophellitol cyclosulfates: a new class of irreversible glycosidase inhibitor. *ACS Cent Sci* **3**: 784-793
- Boisson M, Gomord V, Audran C, Berger N, Dubreucq B, Granier F, Lerouge P, Faye L, Caboche M, Lepiniec L (2001) Arabidopsis glycosidase I mutants reveal a critical role in N-glycan trimming in seed development. *EMBO J.* **20**: 1010-1019
- Cappelli C (1994) Occurrence of *Fusarium oxysporum* f. sp. *gladioli* on saffron in Italy. *Phytopathol. Mediterr.* **33**: 93-94
- Carrascosa JM, Molero JC, Fermin Y, Martinez C, Andres A, Satrustegui J (2001) Effects of chronic treatment with acarbose on glucose and lipid metabolism in obese diabetic Wistar rats. *Diab Obes Metab* **3**: 240-248
- Chandrasekar B, Colby T, Emon AEK, Jiang J, Hong TN, Villamor JG, Harzen A, Overkleeft HS., Van der Hoorn RAL (2014) Broad range glycosidase activity profiling. *Mol Cell Proteomics* **13**: 2787-2800
- Chandrasekar B, Hong TN, Van der Hoorn RAL (2017) Inhibitor discovery by convolution ABPP. *Meth Mol Biol* **1491**: 47-56
- Costantino HR, Brown SH, Kelly RM (1990) Purification and characterization of an α -glucosidase from a hyperthermophilic Archaeobacterium, *Pyrococcus furiosus*, exhibiting a temperature optimum of 105 to 115°C. *J Bacteriol* **172**: 3654-3660
- Coutinho PM, Henrissat B (1999) Carbohydrate-active enzymes: an integrated approach. In: Recent Advances in Carbohydrate Engineering. Edited by Gilbert HJ, Davies GJ, Svensson B, Henrissat B. Royal Society of Chemistry; **1999**: 3-12
- Cox J, Hein MY, Luber CA, Paron I, Nagaraj N, Mann M (2014) Accurate Proteome-wide Label-free Quantification by Delayed Normalization and Maximal Peptide Ratio Extraction, Termed MaxLFQ. *Mol Cell Proteomics* **13**: 2513-2526
- Cox J, Mann M (2008) MaxQuant enables high peptide identification rates, individualized p.p.b.-range mass accuracies and proteome-wide protein quantification. *Nat Biotechnol* **26**: 1367-1372
- Cox J, Neuhauser N, Michalski A, Scheltema RA, Olsen JV, Mann M (2011) Andromeda: a peptide search engine integrated into the MaxQuant environment. *J Proteome Res* **10**: 1794-1805
- Cravatt BF, Wright AT, Kozarich JW (2008) Activity-based protein profiling: from enzyme chemistry to proteomic chemistry. *Ann Rev Biochem* **77**: 383-414
- Finn RD, Coghill P, Eberhardt RY, Eddy SR, Mistry J, Mitchell AL, Potter SC, Punta M, Qureshi M, Sangrador-Vegas A, Salazar GA, Tate J, Bateman A (2016) The Pfam protein families database: towards a more sustainable future. *Nucleic Acids Res* **44**: D279-285
- Frandsen TP, Lok F, Mirgorodskaya E, Roepstroff P, Svensson B (2000) Purification, enzymatic characterisation, and nucleotide sequence of a high-isoelectric-point α -glucosidase from barley malt. *Plant Physiol* **123**: 275-286
- Gershater MC, Cummins I, Edwards R (2017) Role of a carboxylesterase in herbicide bioactivation in Arabidopsis thaliana. *J Biol Chem* **282**: 21460-21466
- Gu C, Kolodziejek I, Misas-Villamil JC, Shindo T, Colby T, Verdoes M, Richau KH, Schmidt J, Overkleeft HS, Van der Hoorn RAL (2010) Proteasome activity profiling: a simple, robust and versatile method revealing subunit-selective inhibitors and cytoplasmic, defence-induced proteasome activities. *Plant J* **62**: 160-170

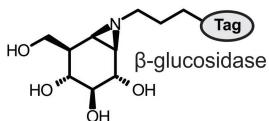
- Gu C, Shannon A, Colby T, Wang Z, Shabab M, Kumari S, Villamor JG, McLaughlin CJ, Weerapana E, Kaiser M, Cravatt BF, Van der Hoorn RAL (2013) Chemical proteomics with sulfonyl fluoride probes reveals selective labeling of functional tyrosines in glutathione transferases. *Chem Biol* **20**: 541-548
- Haas BJ, Papanicolaou A, Yassour M, Grabherr M, Blood PD, Bowden J, Couger MB, Eccles D, Li B, Lieber M, MacManes MD, Ott M, Orvis J, Pochet N, Strozzi F, Weeks N, Westerman R, William T, Dewey CN, Henschel R, LeDuc RD, Friedman N, Regev A (2013) *De novo* transcript sequence reconstruction from RNA-seq using the Trinity platform for reference generation and analysis. *Nat Protoc* **8**: 1494-1512
- Hillman RJ, Scott M, Gray RS (1989) Effect of alpha-glucosidase inhibition on glucose profiles in insulin dependent diabetes. *Diabetes Res* **10**: 81-84
- Hong TN, Van der Hoorn RAL (2014) DIGE-ABPP by click chemistry: pairwise comparison of serine hydrolase activities from the apoplast of infected plants. *Meth Mol Biol* **1127**: 183-194
- Husaini AM (2014) Challenges of climate change – omics-based biology of saffron plants and organic agricultural biotechnology for sustainable saffron production. *GM Crops Food* **5**: 970105
- Hyatt D, Chen GL, Locascio PF, Land ML, Larimer FW, Hauser LJ (2010) Prodigal: prokaryotic gene recognition and translation initiation site identification. *BMC Bioinformatics* **11**: 119
- Iglesias N, Abelenda JA, Rodino M, Sampedro J, Revilla G, Zarra I (2006) Apoplastic glycosidases active against xyloglucan oligosaccharides of *Arabidopsis thaliana*. *Plant Cell Physiol* **47**: 55-63
- Jain M, Srivastava PL, Verma M, Ghangal R, Garg R (2016) *De novo* transcriptome assembly and comprehensive expression profiling in *Crocus sativus* to gain insights into apocarotenoid biosynthesis. *Sci Rep* **6**: 22456
- Jiang J, Kuo, CL, Wu L, Franke C, Kallemijn WW, Florea BI, Van Meel E, Van der Marel G, Codee JDC, Boot RG, Davies GJ, Overkleeft HS, Aerts, JMFG (2016) Detection of active mammalian GH31 α -glucosidases in health and disease using in-class, broad-spectrum activity-based probes. *ACS Cent Sci* **2**: 351-358
- Kallemijn WW, Li KY, Witte MD, Marques ARA, Aten J, Scheij S, Jiang JB, Willems LI, Voorn-Brouwer TM, van Roomen CPAA, Ottenhoff R, Boot RG, van den Elst H, Walvoort, MTC, Florea BI, Codee JDC, van der Marel GA, Aerts JMFG, Overkleeft HS (2012) Novel activity-based probes for broad-spectrum profiling of retaining beta-exoglucosidases *in situ* and *in vivo*. *Angew Chem* **51**: 12529–12533
- Kaschani F, Gu C, Niessen S, Hoover H, Cravatt BF, Van der Hoorn RAL (2009) Diversity of Serine hydrolase activities of non-challenged and Botrytis-infected *Arabidopsis thaliana*. *Mol Cell Proteomics* **8**: 1082-1093
- Kolodziejek I, Misas-Villamil, JC, Kaschani F, Clerc J, Gu C, Krahn D, Niessen S, Verdoes M, Willems LI, Overkleeft HS, Kaiser M, Van der Hoorn RAL (2011) Proteasome activity imaging and profiling characterizes bacterial effector Syringolin A. *Plant Physiol* **155**: 477-489
- Krammer G, Winterhalter P, Schwab M, Shreier P (2002) Glycosidically bound aroma compounds in the fruits of *Prunus* species: apricot (*P. armeniaca* L.), peach (*P. persica* L.), (*P. domestica* L. ssp. *Syriaca*). *Postharvest Biol Technol* **39**: 778-781
- Lenger J, Kaschani F, Lenz T, Dalhoff C, Villamor JG, Koster H, Sewald N, Van der Hoorn RAL (2012) Labeling and enrichment of *Arabidopsis thaliana* matrix metalloproteases using an active-site directed, marimastat-based photoreactive probe. *Bioorg Med Chem* **20**: 592-596
- Lombard V, Golaconda Ramulu H, Drula E, Coutinho PM, Henrissat B (2014) The carbohydrate-active enzymes database (CAZy) in 2013. *Nucl Acids Res* **42**: D490-495
- Lu H, Chandrasekar B, Oeljeklaus J, Misas-Villamil JC, Wang Z, Shindo T, Bogyo M, Kaiser M, Van der Hoorn RAL (2015) Subfamily-specific probes for Cys proteases display dynamic protease activities during seed germination. *Plant Physiol* **168**: 1462-1475

- Martinez DE, Bartoli CG, Grbic V, Guamet JJ** (2007) Vacuolar cysteine proteases of wheat (*Triticum aestivum* L.) are common to leaf senescence induced by different factors. *J Exp Bot* **58**: 1099-1107.
- Michalski A, Damoc E, Lange O, Denisov E, Nolting D, Müller M, Viner R, Schwartz J, Remes P, Belford M, Dunyach JJ, Cox J, Horning S, Mann M, Makarov A** (2012) Ultra high resolution linear ion trap Orbitrap mass spectrometer (Orbitrap Elite) facilitates top down LC MS/MS and versatile peptide fragmentation modes. *Mol Cell Proteomics* **11**: O111 013698
- Misas-Villamil JC, Toenges G, Kolodziejek I, Sadaghiani AM, Kaschani F, Colby T, Bogyo M, Van der Hoorn RAL** (2013) Activity profiling of vacuolar processing enzymes reveals a role for VPE during oomycete infection. *Plant J* **73**: 689-700
- Misas-Villamil JC, Van der Burgh A, Grosse-Holz F, Bach-Pages M, Kaschani F, Schilasky S, Emon AEK, Ruben M, Kaiser M, Overkleeft HS, Van der Hoorn RAL** (2017) Subunit-selective proteasome activity profiling uncovers uncoupled proteasome subunit activities during bacterial infections. *Plant J* **90**: 418-430
- Mohamed MSM, Saleh AM, Abdel-Farid IB, El-Naggar SA** (2017) Growth, hydrolases and ultrastructure of *Fusarium oxysporum* as affected by phenolic rich extracts from several xerophytic plants. *Pesticide Biochem Physiol* **141**: 57-64
- Monroe JD, Gough CM, Chandler LE, Loch CM, Ferrante JE, Wright PW** (1999) Structure, properties and tissue localization of apoplastic α -glucosidase in crucifers. *Plant Physiol* **119**: 385-397
- Morimoto K, Van der Hoorn RAL** (2016) The increasing impact of activity-based protein profiling in plant science. *Plant Cell Physiol* **57**: 446-461
- Mueller AN, Ziemann S, Treitschke S, Aßmann D, Doehlemann G** (2013) Compatibility in the *Ustilago maydis*-maize interaction requires inhibition of host cysteine proteases by the fungal effector Pit2. *PLoS Pathog* **9**: e1003177
- Olsen JV, de Godoy LM, Li G, Macek B, Mortensen P, Pesch R, Makarov A, Lange O, Horning S, Mann M** (2005) Parts per million mass accuracy on an Orbitrap mass spectrometer via lock mass injection into a C-trap. *Mol Cell Proteomics* **4**: 2010-2021
- Palmero D, Rubio-Moraga A, Galvez-Paron L, Nogueras J, Abato C, Gomez-Gomez L, Ahrazem O** (2014) Pathogenicity and genetic diversity of *Fusarium oxysporum* isolates from corms of *Crocus sativus*. *Ind Crops Prod* **61**: 186-192
- Richau K, Kaschani F, Verdoes M, Pansuriya TC, Niessen S, Stüber K, Overkleeft HS, Bogyo M, Van der Hoorn RAL** (2012) Subclassification and biochemical analysis of plant papain-like cysteine proteases displays subfamily-specific characteristics. *Plant Physiol* **158**: 1583-1599
- Sadler NC, Wright AT** (2015) Activity-based protein profiling of microbes. *Curr Opin Chem Biol* **24**: 139-144
- Stanley D, Rejzek M, Naested H, Smedley M, Otero S, Fahy B, Thorpe F, Nash RJ, Harwood W, Svensson B, Denyer K, Field RA, Smith AM** (2011) The role of α -glucosidase in germinating barley grains. *Plant Physiol* **155**: 932-943
- Stiti N, Chandrasekar B, Strubl L, Mohammed S, Bartels D, Van der Hoorn RAL** (2016) Nicotinamide cofactors suppress active-site labeling of aldehyde dehydrogenases. *ACS Chem Biol* **11**: 1578-1586
- Tang S, Lomsadze A, Borodovsky M** (2015) Identification of protein coding regions in RNA transcripts. *Nucl Acid Res* **43**: e78
- Teper-Bamnolker P, Buskila Y, Belausov E, Wolf D, Doron-Faigenboim A, Ben-Dor S, Van der Hoorn RAL, Lers A, Eshel D** (2017) Vacuolar processing enzyme (VPE) activates programmed cell death in the apical meristem inducing loss of apical dominance. *Plant Cell Environ* **40**: 2381-2392
- Tyanova S, Temu T, Sinitcyn P, Carlson A, Hein MY, Geiger T, Mann M, Cox J** (2016) The Perseus computational platform for comprehensive analysis of (prote)omics data. *Nat. Methods* **13**: 731-740
- Verhelst SH, Bogyo M** (2005) Chemical proteomics applied to target identification and drug discovery. *Biotechnol* **38**: 175-177

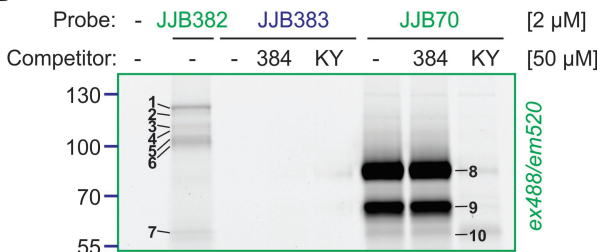
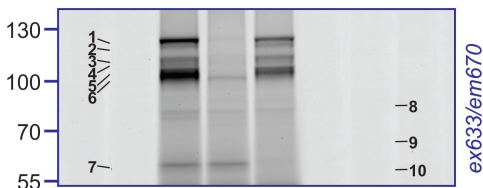
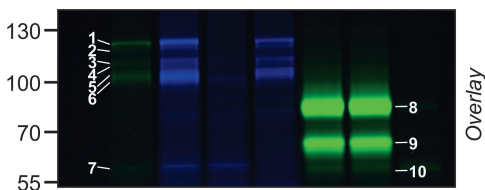
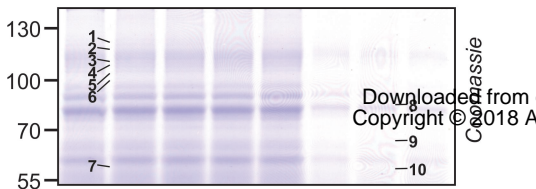
- 888 **Vizcaíno JA, Csordas A, del-Toro N, Dianas JA, Griss J, Lavidas I, Mayer G, Perez-**
889 **Riverol Y, Reisinger F, Ternent T, Xu QW, Wang R, Hermjakob H** (2016) 2016 update
890 of the PRIDE database and related tools. *Nucleic Acids Res* **44**: D447-D456
- 891 **Wafai AH, Bukhari S, Mokhdoomi TA, Amin A, Wani Z, Husaini AM, Mir JI, Qadri**
892 **RA** (2015) Comparative expression analysis of senescence gene *CsNAP* and B-class floral
893 development gene *CsAP3* during different stages of flower development in Saffron (*Crocus*
894 *sativus* L.). *Physiol Mol Biol Plants* **21**: 459-463
- 895 **Wennekes T, Meijer AJ, Groen AK, Boot RG, Groener JE, van Eijk M, Ottenhoff R,**
896 **Bijl N, Ghauharali K, Song H, O'Shea TJ, Liu H, Yew N, Copeland D, van den Berg**
897 **RJ, van der Marel GA, Overkleeft HS, Aerts JM** (2010) Dual-action lipophilic
898 iminosugar improves glycemic control in obese rodents by reduction of visceral
899 glycosphingolipids and buffering of carbohydrate assimilation. *J Med Chem.* **53**: 689-698
- 900 **Wennekes T, van den Berg RJ, Donker W, van der Marel GA, Strijland A, Aerts JM,**
901 **Overkleeft HS** (2007) Development of adamantan-1-yl-methoxy-functionalized 1-
902 deoxynojirimycin derivatives as selective inhibitors of glucosylceramide metabolism in man.
903 *J Org Chem.* **72**: 1088-1097. **Wessel D, Flügge UI** (1984) A method for the quantitative
904 recovery of protein in dilute solution in the presence of detergents and lipids. *Anal Biochem.*
905 **138**: 141-143
- 906 **Willems LI, Overkleeft HS, van Kasteren SI** (2014) Current developments in activity-based
907 protein profiling. *Bioconjug Chem* **25**: 1181-1191
- 908 **Xiao J, Ohshima A, Kamakura T, Ishiyama T, Yamaguchi I** (1994) Extracellular
909 glycoprotein(s) associated with cellular differentiation in *Magnaporthe grisea*. *Mol Plant-*
910 *Microbe Interact* **7**: 639-644

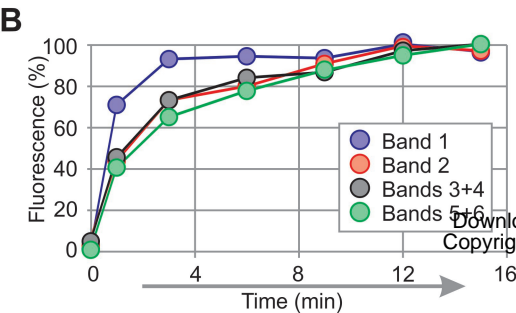
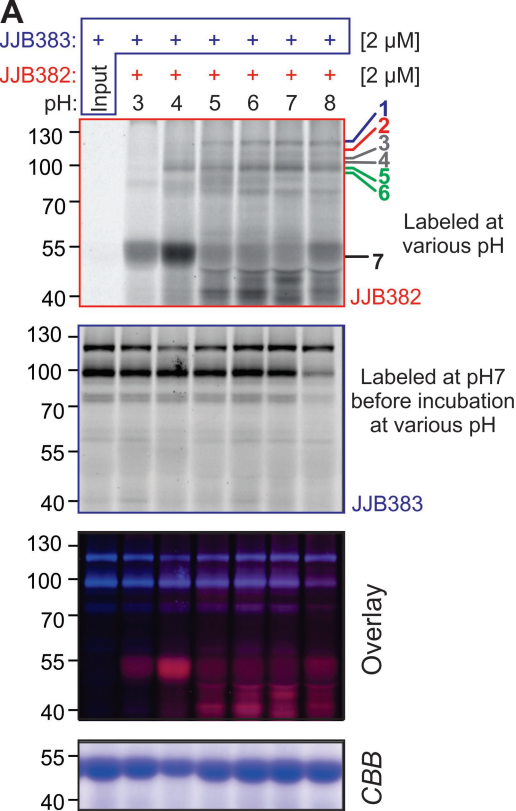
A

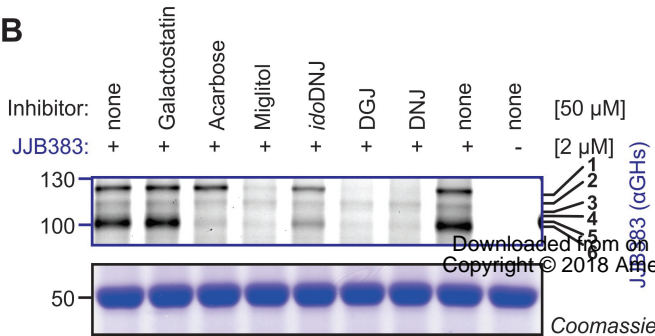
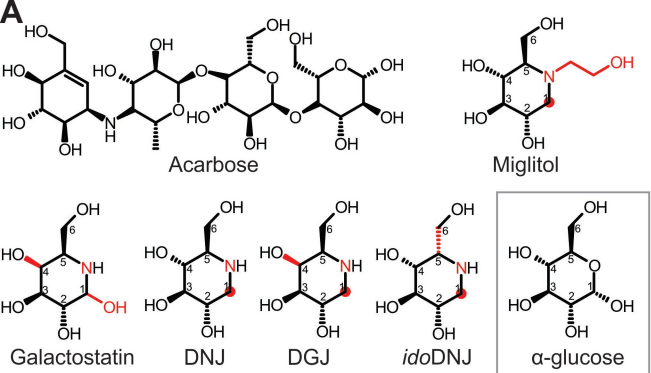
Probe	Tag
JJB382	Bodipy(FL)
JJB383	Cy5
JJB384	Biotin

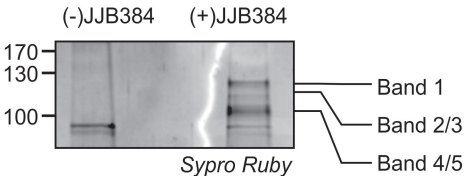


Probe	Tag
KY371	Alkyne
JJB70	Bodipy(FL)
JJB75	Bodipy(TMR)
JJB111	Biotin

B**C****D****E**





A**B**

Spectral counts

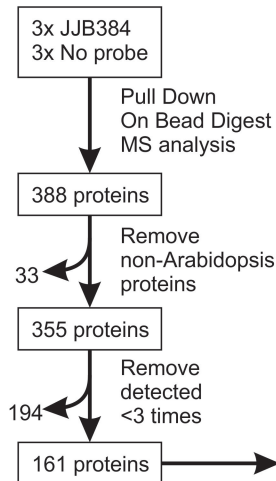
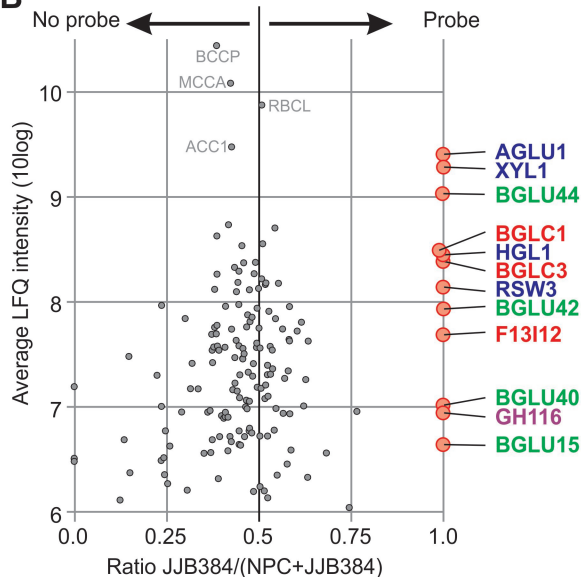
RSW3 **XYL1** **HGL1** **AGLU1** **BGLC3**

13	5	4	3	0
11	6	4	3	0
12	6	4	4	2

C

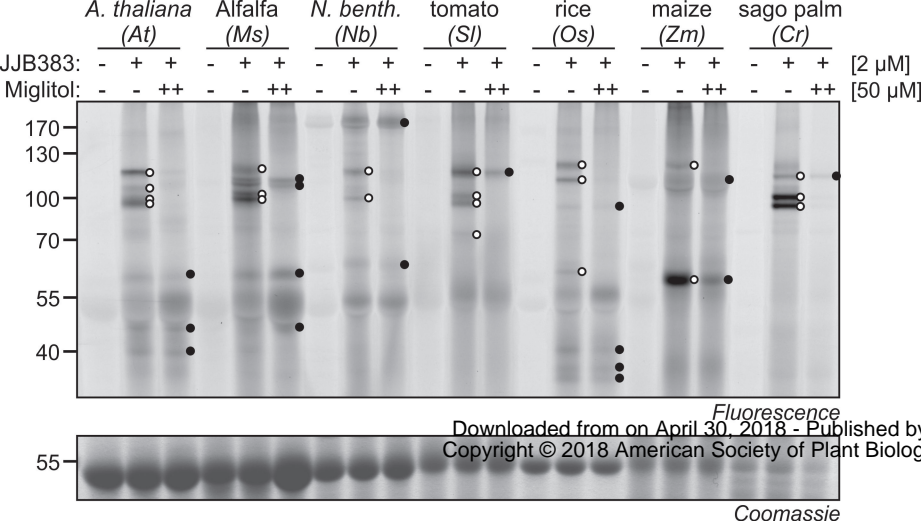
ATG acc.	Name	SP	Protein domains	MW	PGS
At5g11720	AGLU1			101	9
At5g63840	RSW3			104	2
At3g23640	HGL1			111	9
At1g68560	XYL1			102	9
At5g04885	BGLC3		100aa	68	5

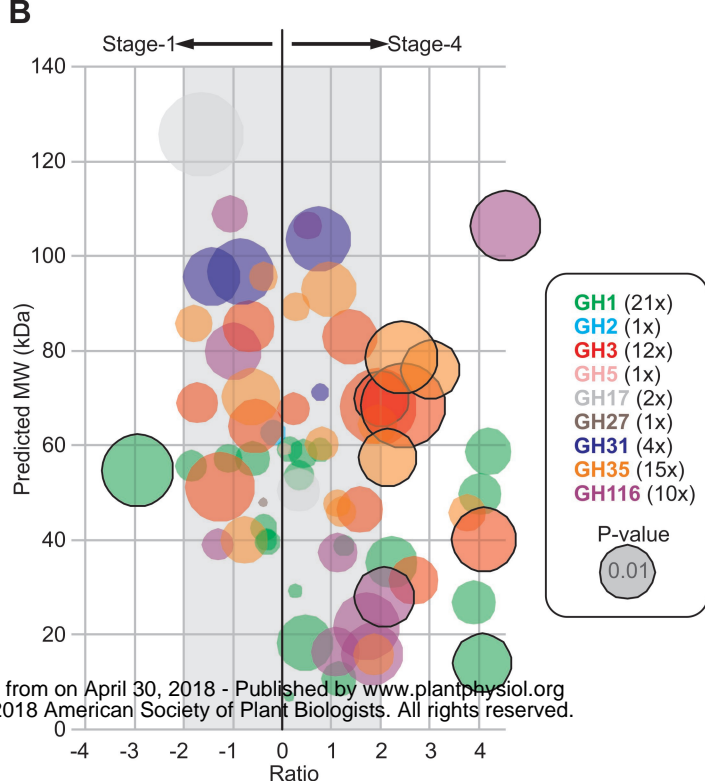
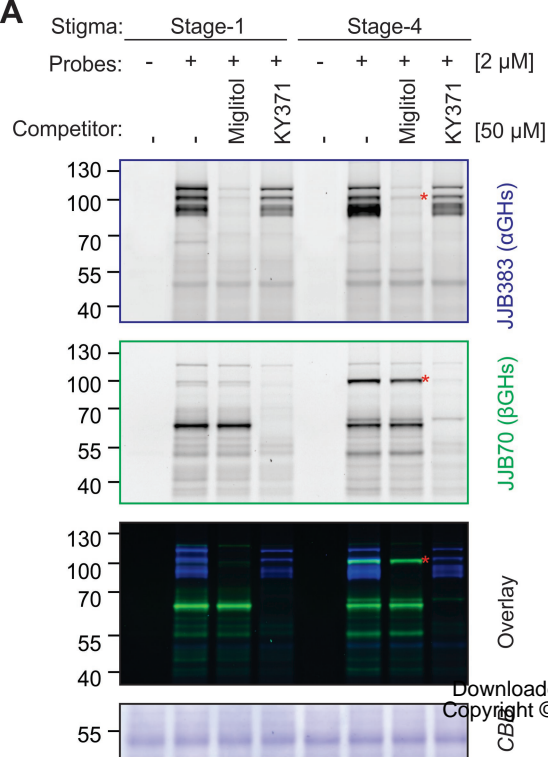
Downloaded from on Ap
Copyright © 2018 Americ

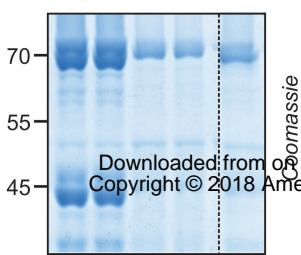
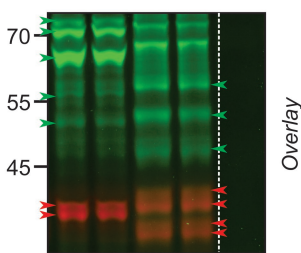
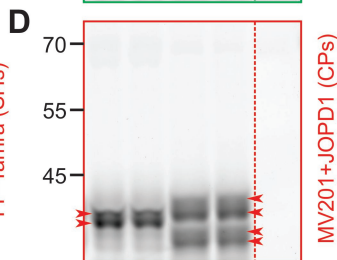
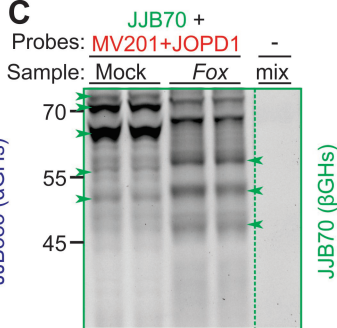
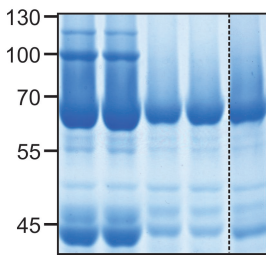
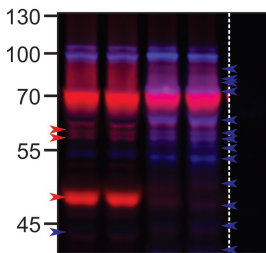
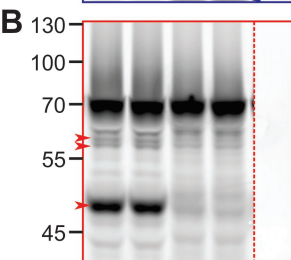
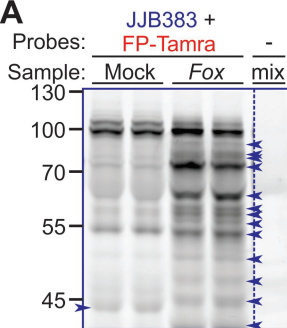
A**B****C**

ATG acc.	Name	SP	Protein domains and peptide coverage	Peptides u a	MW	PGS	JJB11
At5g11720	AGLU1		GH31	39 1	101	9	-
At5g63840	RSW3		GH31	20 0	104	2	-
At3g23640	HGL1		GH31	24 0	111	3	-
At1g68560	XYL1		GH31	32 6	102	9	-
At4g10060	GH116		GH116	11 1	104	4	-
At2g44450	BGLU15		GH1	1 2	57	4	+
At1g26560	BGLU40		GH1	9 0	58	4	+
At5g36890	BGLU42		GH1	16 0	56	1	+
At3g18080	BGLU44		GH1	30 5	59	4	+
At3g47000	F13I12		GH3 GH3	14 4	66	2	+
At5g20950	BGLC1		GH3 GH3	36 0	72	4	+
At5g04885	BGLC3		GH3 GH3	15 0	68	5	+

Peptides: — unique — ambiguous |—| 100aa







Parsed Citations

Andriotis VME, Rejzek M, Barclay E, Rugen MD, Field RA, Smith AM (2017) Cell wall degradation is required for normal starch mobilisation in barley endosperm. *Sci. Rep.* 6: 33215

Pubmed: [Author and Title](#)

CrossRef: [Author and Title](#)

Google Scholar: [Author Only](#) [Title Only](#) [Author and Title](#)

Ahrazem O, Rubio-Moraga A, Nebauer SG, Molina RV, Gómez-Gómez L (2015) Saffron: its phytochemistry, developmental processes, and biotechnological prospects. *J Agric Food Chem* 63: 8751-8764

Pubmed: [Author and Title](#)

CrossRef: [Author and Title](#)

Google Scholar: [Author Only](#) [Title Only](#) [Author and Title](#)

Artola M, Wu L, Ferraz MJ, Kuo CL, Raich L, Breen IZ, Offen WA, Codee JDC, Van der Marel G, Rovira C, Aerts JMFG, Davies GJ and Overkleeft HS (2017) 1,6-cyclophellitol cyclosulfates: a new class of irreversible glycosidase inhibitor. *ACS Cent Sci* 3: 784-793

Pubmed: [Author and Title](#)

CrossRef: [Author and Title](#)

Google Scholar: [Author Only](#) [Title Only](#) [Author and Title](#)

Boisson M, Gomord V, Audran C, Berger N, Dubreucq B, Granier F, Lerouge P, Faye L, Caboche M, Lepiniec L (2001) Arabidopsis glycosidase I mutants reveal a critical role in N-glycan trimming in seed development. *EMBO J.* 20: 1010-1019

Pubmed: [Author and Title](#)

CrossRef: [Author and Title](#)

Google Scholar: [Author Only](#) [Title Only](#) [Author and Title](#)

Cappelli C (1994) Occurrence of *Fusarium oxysporum* f. sp. *gladioli* on saffron in Italy. *Phytopathol. Mediterr.* 33: 93-94

Pubmed: [Author and Title](#)

CrossRef: [Author and Title](#)

Google Scholar: [Author Only](#) [Title Only](#) [Author and Title](#)

Carrascosa JM, Molero JC, Fermin Y, Martinez C, Andres A, Satrustegui J (2001) Effects of chronic treatment with acarbose on glucose and lipid metabolism in obese diabetic Wistar rats. *Diab Obes Metab* 3: 240-248

Pubmed: [Author and Title](#)

CrossRef: [Author and Title](#)

Google Scholar: [Author Only](#) [Title Only](#) [Author and Title](#)

Chandrasekar B, Colby T, Emon AEK, Jiang J, Hong TN, Villamor JG, Harzen A, Overkleeft HS., Van der Hoorn RAL (2014) Broad range glycosidase activity profiling. *Mol Cell Proteomics* 13: 2787-2800

Pubmed: [Author and Title](#)

CrossRef: [Author and Title](#)

Google Scholar: [Author Only](#) [Title Only](#) [Author and Title](#)

Chandrasekar B, Hong TN, Van der Hoorn RAL (2017) Inhibitor discovery by convolution ABPP. *Meth Mol Biol* 1491: 47-56

Pubmed: [Author and Title](#)

CrossRef: [Author and Title](#)

Google Scholar: [Author Only](#) [Title Only](#) [Author and Title](#)

Costantino HR, Brown SH, Kelly RM (1990) Purification and characterization of an α -glucosidase from a hyperthermophilic Archaeobacterium, *Pyrococcus furiosus*, exhibiting a temperature optimum of 105 to 115°C. *J Bacteriol* 172: 3654-3660

Pubmed: [Author and Title](#)

CrossRef: [Author and Title](#)

Google Scholar: [Author Only](#) [Title Only](#) [Author and Title](#)

Coutinho PM, Henrissat B (1999) Carbohydrate-active enzymes: an integrated approach. In: *Recent Advances in Carbohydrate Engineering*. Edited by Gilbert HJ, Davies GJ, Svensson B, Henrissat B. Royal Society of Chemistry, 1999: 3-12

Pubmed: [Author and Title](#)

CrossRef: [Author and Title](#)

Google Scholar: [Author Only](#) [Title Only](#) [Author and Title](#)

Cox J, Hein MY, Lubner CA, Paron I, Nagaraj N, Mann M (2014) Accurate Proteome-wide Label-free Quantification by Delayed Normalization and Maximal Peptide Ratio Extraction, Termed MaxLFQ. *Mol Cell Proteomics* 13: 2513-2526

Pubmed: [Author and Title](#)

CrossRef: [Author and Title](#)

Google Scholar: [Author Only](#) [Title Only](#) [Author and Title](#)

Cox J, Mann M (2008) MaxQuant enables high peptide identification rates, individualized p.p.b.-range mass accuracies and proteome-wide protein quantification. *Nat Biotechnol* 26: 1367-1372

Pubmed: [Author and Title](#)

CrossRef: [Author and Title](#)

Google Scholar: [Author Only](#) [Title Only](#) [Author and Title](#)

Cox J, Neuhauser N, Michalski A, Scheltema RA, Olsen JV, Mann M (2011) Andromeda: a peptide search engine integrated into the MaxQuant environment. *J Proteome Res* 10: 1794-1805

Pubmed: [Author and Title](#)
CrossRef: [Author and Title](#)
Google Scholar: [Author Only Title Only Author and Title](#)

Cravatt BF, Wright AT, Kozarich JW (2008) Activity-based protein profiling: from enzyme chemistry to proteomic chemistry. *Ann Rev Biochem* 77: 383-414

Pubmed: [Author and Title](#)
CrossRef: [Author and Title](#)
Google Scholar: [Author Only Title Only Author and Title](#)

Finn RD, Coghill P, Eberhardt RY, Eddy SR, Mistry J, Mitchell AL, Potter SC, Punta M, Qureshi M, Sangrador-Vegas A, Salazar GA, Tate J, Bateman A (2016) The Pfam protein families database: towards a more sustainable future. *Nucleic Acids Res* 44: D279-285

Pubmed: [Author and Title](#)
CrossRef: [Author and Title](#)
Google Scholar: [Author Only Title Only Author and Title](#)

Frandsen TP, Lok F, Mirgorodskaya E, Roepstroff P, Svensson B (2000) Purification, enzymatic characterisation, and nucleotide sequence of a high-isoelectric-point α -glucosidase from barley malt. *Plant Physiol* 123: 275-286

Pubmed: [Author and Title](#)
CrossRef: [Author and Title](#)
Google Scholar: [Author Only Title Only Author and Title](#)

Gershater MC, Cummins I, Edwards R (2017) Role of a carboxylesterase in herbicide bioactivation in *Arabidopsis thaliana*. *J Biol Chem* 282: 21460-21466

Pubmed: [Author and Title](#)
CrossRef: [Author and Title](#)
Google Scholar: [Author Only Title Only Author and Title](#)

Gu C, Kolodziejek I, Misas-Villamil JC, Shindo T, Colby T, Verdoes M, Richau KH, Schmidt J, Overkleeft HS, Van der Hoorn RAL (2010) Proteasome activity profiling: a simple, robust and versatile method revealing subunit-selective inhibitors and cytoplasmic, defence-induced proteasome activities. *Plant J* 62: 160-170

Pubmed: [Author and Title](#)
CrossRef: [Author and Title](#)
Google Scholar: [Author Only Title Only Author and Title](#)

Gu C, Shannon A, Colby T, Wang Z, Shabab M, Kumari S, Villamor JG, McLaughlin CJ, Weerapana E, Kaiser M, Cravatt BF, Van der Hoorn RAL (2013) Chemical proteomics with sulfonyl fluoride probes reveals selective labeling of functional tyrosines in glutathione transferases. *Chem Biol* 20: 541-548

Pubmed: [Author and Title](#)
CrossRef: [Author and Title](#)
Google Scholar: [Author Only Title Only Author and Title](#)

Haas BJ, Papanicolaou A, Yassour M, Grabherr M, Blood PD, Bowden J, Couger MB, Eccles D, Li B, Lieber M, MacManes MD, Ott M, Orvis J, Pochet N, Strozzi F, Weeks N, Westerman R, William T, Dewey CN, Henschel R, LeDuc RD, Friedman N, Regev A (2013) De novo transcript sequence reconstruction from RNA-seq using the Trinity platform for reference generation and analysis. *Nat Protoc* 8: 1494-1512

Pubmed: [Author and Title](#)
CrossRef: [Author and Title](#)
Google Scholar: [Author Only Title Only Author and Title](#)

Hillman RJ, Scott M, Gray RS (1989) Effect of alpha-glucosidase inhibition on glucose profiles in insulin dependent diabetes. *Diabetes Res* 10: 81-84

Pubmed: [Author and Title](#)
CrossRef: [Author and Title](#)
Google Scholar: [Author Only Title Only Author and Title](#)

Hong TN, Van der Hoorn RAL (2014) DIGE-ABPP by click chemistry: pairwise comparison of serine hydrolase activities from the apoplast of infected plants. *Meth Mol Biol* 1127: 183-194

Pubmed: [Author and Title](#)
CrossRef: [Author and Title](#)
Google Scholar: [Author Only Title Only Author and Title](#)

Husaini AM (2014) Challenges of climate change – omics-based biology of saffron plants and organic agricultural biotechnology for sustainable saffron production. *GM Crops Food* 5: 970105

Pubmed: [Author and Title](#)
CrossRef: [Author and Title](#)
Google Scholar: [Author Only Title Only Author and Title](#)

Hyatt D, Chen GL, Locascio PF, Land ML, Larimer FW, Hauser LJ (2010) Prodigal: prokaryotic gene recognition and translation initiation site identification. *BMC Bioinformatics* 11: 119

Pubmed: [Author and Title](#)
CrossRef: [Author and Title](#)
Google Scholar: [Author Only Title Only Author and Title](#)

Iglesias N, Abelenda JA, Rodino M, Sampedro J, Revilla G, Zarra I (2006) Apoplastic glycosidases active against xyloglucan

oligosaccharides of *Arabidopsis thaliana*. Plant Cell Physiol 47: 55-63

Pubmed: [Author and Title](#)

CrossRef: [Author and Title](#)

Google Scholar: [Author Only](#) [Title Only](#) [Author and Title](#)

Jain M, Srivastava PL, Verma M, Ghangal R, Garg R (2016) De novo transcriptome assembly and comprehensive expression profiling in *Crocus sativus* to gain insights into apocarotenoid biosynthesis. Sci Rep 6: 22456

Pubmed: [Author and Title](#)

CrossRef: [Author and Title](#)

Google Scholar: [Author Only](#) [Title Only](#) [Author and Title](#)

Jiang J, Kuo, CL, Wu L, Franke C, Kallemeijn WW, Florea BI, Van Meel E, Van der Marel G, Codee JDC, Boot RG, Davies GJ, Overkleeft HS, Aerts, JMFG (2016) Detection of active mammalian GH31 α -glucosidases in health and disease using in-class, broad-spectrum activity-based probes. ACS Cent Sci 2: 351-358

Pubmed: [Author and Title](#)

CrossRef: [Author and Title](#)

Google Scholar: [Author Only](#) [Title Only](#) [Author and Title](#)

Kallemeijn WW, Li KY, Witte MD, Marques ARA, Aten J, Scheij S, Jiang JB, Willems LI, Voorn-Brouwer TM, van Roomen CPAA, Ottenhoff R, Boot RG, van den Elst H, Walvoort, MTC, Florea BI, Codee JDC, van der Marel GA, Aerts JMFG, Overkleeft HS (2012) Novel activity-based probes for broad-spectrum profiling of retaining beta-exoglucosidases in situ and in vivo. Angew Chem 51: 12529–12533

Pubmed: [Author and Title](#)

CrossRef: [Author and Title](#)

Google Scholar: [Author Only](#) [Title Only](#) [Author and Title](#)

Kaschani F, Gu C, Niessen S, Hoover H, Cravatt BF, Van der Hoorn RAL (2009) Diversity of Serine hydrolase activities of non-challenged and Botrytis-infected *Arabidopsis thaliana*. Mol Cell Proteomics 8: 1082-1093

Pubmed: [Author and Title](#)

CrossRef: [Author and Title](#)

Google Scholar: [Author Only](#) [Title Only](#) [Author and Title](#)

Kolodziejek I, Misas-Villamil, JC, Kaschani F, Clerc J, Gu C, Krahn D, Niessen S, Verdoes M, Willems LI, Overkleeft HS, Kaiser M, Van der Hoorn RAL (2011) Proteasome activity imaging and profiling characterizes bacterial effector Syringolin A Plant Physiol 155: 477-489

Pubmed: [Author and Title](#)

CrossRef: [Author and Title](#)

Google Scholar: [Author Only](#) [Title Only](#) [Author and Title](#)

Krammer G, Winterhalter P, Schwab M, Shreier P (2002) Glycosidically bound aroma compounds in the fruits of *Prunus* species: apricot (*P. armeniaca* L.), peach (*P. persica* L.), (*P. domestica* L. ssp. *Syriaca*). Postharvest Biol Technol 39: 778-781

Pubmed: [Author and Title](#)

CrossRef: [Author and Title](#)

Google Scholar: [Author Only](#) [Title Only](#) [Author and Title](#)

Lenger J, Kaschani F, Lenz T, Dalhoff C, Villamor JG, Koster H, Sewald N, Van der Hoorn RAL (2012) Labeling and enrichment of *Arabidopsis thaliana* matrix metalloproteases using an active-site directed, marimastat-based photoreactive probe. Bioorg Med Chem 20: 592-596

Pubmed: [Author and Title](#)

CrossRef: [Author and Title](#)

Google Scholar: [Author Only](#) [Title Only](#) [Author and Title](#)

Lombard V, Golaconda Ramulu H, Drula E, Coutinho PM, Henrissat B (2014) The carbohydrate-active enzymes database (CAZy) in 2013. Nucl Acids Res 42: D490-495

Pubmed: [Author and Title](#)

CrossRef: [Author and Title](#)

Google Scholar: [Author Only](#) [Title Only](#) [Author and Title](#)

Lu H, Chandrasekar B, Oeljeklaus J, Misas-Villamil JC, Wang Z, Shindo T, Bogyo M, Kaiser M, Van der Hoorn RAL (2015) Subfamily-specific probes for Cys proteases display dynamic protease activities during seed germination. Plant Physiol 168: 1462-1475

Pubmed: [Author and Title](#)

CrossRef: [Author and Title](#)

Google Scholar: [Author Only](#) [Title Only](#) [Author and Title](#)

Martinez DE, Bartoli CG, Grbic V, Guamet JJ (2007) Vacuolar cysteine proteases of wheat (*Triticum aestivum* L.) are common to leaf senescence induced by different factors. J Exp Bot 58: 1099-1107.

Pubmed: [Author and Title](#)

CrossRef: [Author and Title](#)

Google Scholar: [Author Only](#) [Title Only](#) [Author and Title](#)

Michalski A, Damoc E, Lange O, Denisov E, Nolting D, Müller M, Viner R, Schwartz J, Remes P, Belford M, Dunyach JJ, Cox J, Horning S, Mann M, Makarov A (2012) Ultra high resolution linear ion trap Orbitrap mass spectrometer (Orbitrap Elite) facilitates top down LC MS/MS and versatile peptide fragmentation modes. Mol Cell Proteomics 11: O111 013698

Pubmed: [Author and Title](#)

CrossRef: [Author and Title](#)

Google Scholar: [Author Only](#) [Title Only](#) [Author and Title](#)

Misas-Villamil JC, Toenges G, Kolodziejek I, Sadaghiani AM, Kaschani F, Colby T, Bogyo M, Van der Hoorn RAL (2013) Activity profiling of vacuolar processing enzymes reveals a role for VPE during oomycete infection. Plant J 73: 689-700

Pubmed: [Author and Title](#)

CrossRef: [Author and Title](#)

Google Scholar: [Author Only Title Only Author and Title](#)

Misas-Villamil JC, Van der Burgh A, Grosse-Holz F, Bach-Pages M, Kaschani F, Schilasky S, Emon AEK, Ruben M, Kaiser M, Overkleef HS, Van der Hoorn RAL (2017) Subunit-selective proteasome activity profiling uncovers uncoupled proteasome subunit activities during bacterial infections. Plant J 90: 418-430

Pubmed: [Author and Title](#)

CrossRef: [Author and Title](#)

Google Scholar: [Author Only Title Only Author and Title](#)

Mohamed MSM, Saleh AM, Abdel-Farid IB, El-Naggar SA (2017) Growth, hydrolases and ultrastructure of Fusarium oxysporum as affected by phenolic rich extracts from several xerophytic plants. Pesticide Biochem Physiol 141: 57-64

Pubmed: [Author and Title](#)

CrossRef: [Author and Title](#)

Google Scholar: [Author Only Title Only Author and Title](#)

Monroe JD, Gough CM, Chandler LE, Loch CM, Ferrante JE, Wright PW (1999) Structure, properties and tissue localization of apoplastic α -glucosidase in crucifers. Plant Physiol 119: 385-397

Pubmed: [Author and Title](#)

CrossRef: [Author and Title](#)

Google Scholar: [Author Only Title Only Author and Title](#)

Morimoto K, Van der Hoorn RAL (2016) The increasing impact of activity-based protein profiling in plant science. Plant Cell Physiol 57: 446-461

Pubmed: [Author and Title](#)

CrossRef: [Author and Title](#)

Google Scholar: [Author Only Title Only Author and Title](#)

Mueller AN, Ziemann S, Treitschke S, Aßmann D, Doehlemann G (2013) Compatibility in the Ustilago maydis-maize interaction requires inhibition of host cysteine proteases by the fungal effector Pit2. PLoS Pathog 9: e1003177

Pubmed: [Author and Title](#)

CrossRef: [Author and Title](#)

Google Scholar: [Author Only Title Only Author and Title](#)

Olsen JV, de Godoy LM, Li G, Macek B, Mortensen P, Pesch R, Makarov A, Lange O, Horning S, Mann M (2005) Parts per million mass accuracy on an Orbitrap mass spectrometer via lock mass injection into a C-trap. Mol Cell Proteomics 4: 2010-2021

Pubmed: [Author and Title](#)

CrossRef: [Author and Title](#)

Google Scholar: [Author Only Title Only Author and Title](#)

Palmero D, Rubio-Moraga A, Galvez-Paron L, Noguera J, Abato C, Gomez-Gomez L, Ahrazem O (2014) Pathogenicity and genetic diversity of Fusarium oxysporum isolates from corms of Crocus sativus. Ind Crops Prod 61: 186-192

Pubmed: [Author and Title](#)

CrossRef: [Author and Title](#)

Google Scholar: [Author Only Title Only Author and Title](#)

Richau K, Kaschani F, Verdoes M, Pansuriya TC, Niessen S, Stüber K, Overkleef HS, Bogyo M, Van der Hoorn RAL (2012) Subclassification and biochemical analysis of plant papain-like cysteine proteases displays subfamily-specific characteristics. Plant Physiol 158: 1583-1599

Pubmed: [Author and Title](#)

CrossRef: [Author and Title](#)

Google Scholar: [Author Only Title Only Author and Title](#)

Sadler NC, Wright AT (2015) Activity-based protein profiling of microbes. Curr Opin Chem Biol. 24: 139-144

Pubmed: [Author and Title](#)

CrossRef: [Author and Title](#)

Google Scholar: [Author Only Title Only Author and Title](#)

Stanley D, Rejzek M, Naested H, Smedley M, Otero S, Fahy B, Thorpe F, Nash RJ, Harwood W, Svensson B, Denyer K, Field RA, Smith AM (2011) The role of α -glucosidase in germinating barley grains. Plant Physiol 155: 932-943

Pubmed: [Author and Title](#)

CrossRef: [Author and Title](#)

Google Scholar: [Author Only Title Only Author and Title](#)

Stiti N, Chandrasekar B, Strubl L, Mohammed S, Bartels D, Van der Hoorn RAL (2016) Nicotinamide cofactors suppress active-site labeling of aldehyde dehydrogenases. ACS Chem Biol 11: 1578-1586

Pubmed: [Author and Title](#)

CrossRef: [Author and Title](#)

Google Scholar: [Author Only Title Only Author and Title](#)

Tang S, Lomsadze A, Borodovsky M (2015) Identification of protein coding regions in RNA transcripts. Nucl Acid Res 43: e78

Pubmed: [Author and Title](#)

CrossRef: [Author and Title](#)
Google Scholar: [Author Only](#) [Title Only](#) [Author and Title](#)

Teper-Bamnolker P, Buskila Y, Belausov E, Wolf D, Doron-Faigenboim A, Ben-Dor S, Van der Hoorn RAL, Lers A, Eshel D (2017) Vacuolar processing enzyme (VPE) activates programmed cell death in the apical meristem inducing loss of apical dominance. Plant Cell Environ 40: 2381-2392

Pubmed: [Author and Title](#)
CrossRef: [Author and Title](#)
Google Scholar: [Author Only](#) [Title Only](#) [Author and Title](#)

Tyanova S, Temu T, Sinitcyn P, Carlson A, Hein MY, Geiger T, Mann M, Cox J (2016) The Perseus computational platform for comprehensive analysis of (prote)omics data. Nat. Methods 13: 731-740

Pubmed: [Author and Title](#)
CrossRef: [Author and Title](#)
Google Scholar: [Author Only](#) [Title Only](#) [Author and Title](#)

Verhelst SH, Bogoy M (2005) Chemical proteomics applied to target identification and drug discovery. Biotechnol 38: 175-177

Pubmed: [Author and Title](#)
CrossRef: [Author and Title](#)
Google Scholar: [Author Only](#) [Title Only](#) [Author and Title](#)

Vizcaino JA, Csordas A, del-Toro N, Dienes JA, Griss J, Lavidas I, Mayer G, Perez-Riverol Y, Reisinger F, Ternent T, Xu QW, Wang R, Hermjakob H (2016) 2016 update of the PRIDE database and related tools. Nucleic Acids Res 44: D447-D456

Pubmed: [Author and Title](#)
CrossRef: [Author and Title](#)
Google Scholar: [Author Only](#) [Title Only](#) [Author and Title](#)

Wafai AH, Bukhari S, Mokhdoomi TA, Amin A, Wani Z, Husaini AM, Mir JI, Qadri RA (2015) Comparative expression analysis of senescence gene CsNAP and B-class floral development gene CsAP3 during different stages of flower development in Saffron (Crocus sativus L.). Physiol Mol Biol Plants 21: 459-463

Pubmed: [Author and Title](#)
CrossRef: [Author and Title](#)
Google Scholar: [Author Only](#) [Title Only](#) [Author and Title](#)

Wennekes T, Meijer AJ, Groen AK, Boot RG, Groener JE, van Eijk M, Ottenhoff R, Bijl N, Ghauharali K, Song H, O'Shea TJ, Liu H, Yew N, Copeland D, van den Berg RJ, van der Marel GA, Overkleeft HS, Aerts JM (2010) Dual-action lipophilic iminosugar improves glycemic control in obese rodents by reduction of visceral glycosphingolipids and buffering of carbohydrate assimilation. J Med Chem 53: 689-698

Pubmed: [Author and Title](#)
CrossRef: [Author and Title](#)
Google Scholar: [Author Only](#) [Title Only](#) [Author and Title](#)

Wennekes T, van den Berg RJ, Donker W, van der Marel GA, Strijland A, Aerts JM, Overkleeft HS (2007) Development of adamantan-1-yl-methoxy-functionalized 1-deoxynojirimycin derivatives as selective inhibitors of glucosylceramide metabolism in man. J Org Chem 72: 1088-1097.
Wessel D, Flügge UI (1984) A method for the quantitative recovery of protein in dilute solution in the presence of detergents and lipids. Anal Biochem 138: 141-143

Pubmed: [Author and Title](#)
CrossRef: [Author and Title](#)
Google Scholar: [Author Only](#) [Title Only](#) [Author and Title](#)

Willems LI, Overkleeft HS, van Kasteren SI (2014) Current developments in activity-based protein profiling. Bioconjug Chem 25: 1181-1191

Pubmed: [Author and Title](#)
CrossRef: [Author and Title](#)
Google Scholar: [Author Only](#) [Title Only](#) [Author and Title](#)

Xiao J, Ohshima A, Kamakura T, Ishiyama T, Yamaguchi I (1994) Extracellular glycoprotein(s) associated with cellular differentiation in Magnaporthe grisea. Mol Plant-Microbe Interact 7: 639-644

Pubmed: [Author and Title](#)
CrossRef: [Author and Title](#)
Google Scholar: [Author Only](#) [Title Only](#) [Author and Title](#)